# An Analytical Assessment of Finite Element and Isogeometric Analyses of the Whole Spectrum of Timoshenko Beams

**Antonio Cazzani**[1,*]**, Flavio Stochino**[1,2,**]**, and Emilio Turco**[2,***]

[1] University of Cagliari, DICAAR — Dept. of Civil and Environmental Engineering and Architecture, 2, via Marengo, I–09123 Cagliari, Italy

[2] University of Sassari, DADU — Dept. of Architecture, Design and Urban Planning, Asilo Sella, 35, via Garibaldi, I–07041 Alghero (SS), Italy

The theoretical results relevant to the vibration modes of Timoshenko beams are here used as benchmarks for assessing the correctness of the numerical values provided by several finite element models, based on either the traditional Lagrangian interpolation or on the recently developed isogeometric approach. Comparison of results is performed on both spectrum error (in terms of the detected natural frequencies) and on the $l^2$ relative error (in terms of the computed eigenmodes): this double check allows detecting for each finite element model, and for a discretization based on the *same* number of degrees-of-freedom, $N$, the frequency threshold above which some prescribed accuracy level is lost, and results become more and more unreliable. Hence a quantitative way of measuring the finite element performance in modeling a Timoshenko beam is proposed. The use of Fast Fourier Transform is finally employed, for a selected set of vibration modes, to explain the reasons of the accuracy decay, mostly linked to a poor separation of the natural frequencies in the spectrum, which is responsible of some aliasing of modes.

## 1 Introduction

Several structural models of beams have been proposed in the last two centuries. In particular, four theoretical models can be considered to be of paramount importance for standard structural mechanics applications, when there is no coupling between transversal and longitudinal vibrations and second- or higher-order effects can be neglected. The Euler-Bernoulli [83] model takes into account bending stiffness and transversal inertia: it is very simple but effective in case of thin beam with large span/depth ratio. Bresse [16] and, separately, Lord Rayleigh [85] improved this model considering also rotary inertia, but not shear stiffness. The dual model, labeled shear beam, takes into account shear stiffness, but not rotary inertia. Finally the idea of a beam model capable of taking into account both shear stiffness and rotary inertia was introduced by Timoshenko in 1921 [86] and 1922 [87] and since then it is associated to his name. An interesting comparison among the dynamics behaviors of these models can be found in [50]; a clarifying spectral analysis of coupled Timoshenko and Euler-Bernoulli model is presented in [11]. A thorough critical review of these beam models has been recently proposed by Elishakoff and his coworkers [41].

Often, it is not possible to obtain closed-form solutions for beam vibration problems; in such cases numerical approaches become very important. The development of these methods is still an active area of research, and interesting examples of new approaches are presented in [77].

One of the most effective idea of the last ten years is the so-called isogeometric analysis (IGA). It was introduced by Hughes *et al.* in [53] and is an isoparametric finite element approach based on Non-Uniform Rational Basis Splines (NURBS) shape functions. Its main characteristic is the use of the *same* geometric description obtained by computer aided design (CAD) techniques; for this reason mesh refinement is possible without going back to the CAD model.

In order to test the accuracy of the above mentioned numerical solution of free vibrations problems, the evaluation of the complete frequency spectrum corresponding to an $N$ degrees-of-freedom finite element model is an effective idea. For finite element analysis, early examples have been proposed in [55] and [52]. Similar frequency spectra have been

---

* Corresponding author   E-mail: antonio.cazzani@unica.it, Phone: +39 070 675 5420, Fax: +39 070 675 5418
** E-mail: fstochino@uniss.it
*** E-mail: emilio.turco@uniss.it

constructed for the isogeometric finite element method in [31] and [78]. In these papers the free vibrations of elastic rods, Euler-Bernoulli beams, elastic membranes, Kirchhoff plates, thin circular plates and stiffened cylindrical shells have been investigated, with an interesting comparison between standard and isogeometric finite elements.

Isogeometric models have produced interesting results for several problems of different kind. Ref. [57] presents a vibration analysis of Timoshenko beams, with particular emphasis on refinement schemes. Thanks to their effective geometric description, IGA models have proven to be powerful in case of curved beam for both static ( [21], [20], [22], [27]) and dynamic problems (see [58] for the Timoshenko beam model, and [89] for the Euler-Bernoulli one).

Free vibration analysis of composite beams is another trendy topic in computational mechanics: as meaningful examples, the review work [49], and the analysis presented in [48] should be considered. Isogeometric analysis has proven to be very accurate and convenient also in this case, see *e.g.* the work of Luu *et al.* [59].

Control problems have become very popular nowadays, with particular reference to beam structures and related models. For example in [51] a FEM approach for an optimal control problem involving Timoshenko beams is presented, while the opportunities offered by piezoelectric materials are depicted in [65].

As far as the authors know the complete frequency spectrum for free vibrations of Timoshenko beams has not been studied yet; in particular it seems that a thorough comparison between isogeometric and standard finite elements for this case has not been presented in the literature. For this reason this paper is devoted to this issue, with particular attention to new methods for evaluating the accuracy in eigenmodes estimation.

The rest of the paper is organized as follows: in Section 2 the governing equations of the dynamics for a straight Timoshenko beam are presented (see for details [23], [24]). Discussion is then focused on the eigensolutions: it is shown that the spectrum is composed of two parts divided by a transition frequency which depends only on the ratio between shear stiffness and rotary inertia. Depending on the applied boundary conditions this frequency may be, or may be not, part of the spectrum. Then, in Section 3 modal analysis for the single-span Timoshenko beam model is presented for two representative boundary conditions cases, namely the simply-supported and the doubly clamped beam. In Section 4 the finite element models for Timoshenko beam, based on both the traditional Lagrangian formulation and the isogeometric one are presented in a quite general form. Next, in Section 5, the numerical frequency spectra produced by these finite element models are compared with those resulting from theoretical predictions; in this way a comparison in terms of the predicted and computed frequencies is presented and discussed, similarly to what has been already done, in the literature, for the Euler-Bernoulli beam model. In addition, the accuracy of approximating the eigenmodes is addressed by comparing the relative error between theoretical and computed vibration shapes in a suitable $l^2$ discrete norm. A Fourier analysis has been also employed to investigate the accuracy of the eigenmodes produced by the discrete models. Finally in Section 6 some conclusions are drawn; future developments and possible applications of the present research are exemplified.

## 2    The governing equations of dynamics for Timoshenko beams

For a uniform, straight Timoshenko beam, the constitutive equations in terms of the generalized internal forces, $T$ and $M$ (which stand respectively for the transversal shear force and the bending moment), taking into account that $G$ and $E$ are shear and Young's moduli, $\kappa$, $A$ and $I$ the shear-correction factor, the area and the area moment of inertia of the beam cross-section, read

$$T = G\kappa A \left( \frac{\partial v}{\partial x} + \phi \right), \quad M = EI \frac{\partial \phi}{\partial x}. \tag{1}$$

In Eq. (1) the generalized components of beam displacement, $v = v(x,t)$ and $\phi = \phi(x,t)$, appear; they are respectively the transversal displacement of the centroid and the cross-section rotation, which depend (when dynamic problems are considered) on both the abscissa, $x$, and time, $t$. The adopted positive convention for internal forces and generalized displacement components are shown in Figure 1.

Linear and angular momentum balance equations, written in terms of kinematic variables alone, yield these coupled equations of motion

$$G\kappa A \left( \frac{\partial^2 v}{\partial x^2} + \frac{\partial \phi}{\partial x} \right) - \rho A \frac{\partial^2 v}{\partial t^2} = 0, \tag{2}$$

$$EI \frac{\partial^2 \phi}{\partial x^2} - G\kappa A \left( \frac{\partial v}{\partial x} + \phi \right) - \rho I \frac{\partial^2 \phi}{\partial t^2} = 0. \tag{3}$$

In Eqs. (2)–(3) $\rho$ is the density of the material constituting the beam.
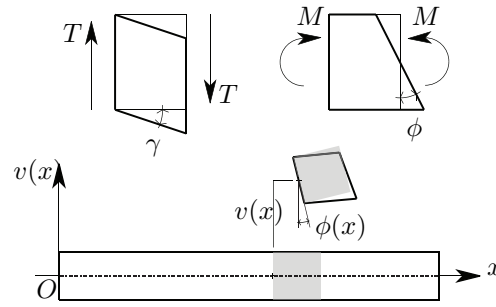
**Fig. 1** Timoshenko beam element showing the assumed conventions for generalized displacements $(v, \phi)$ and internal forces $(T, M)$.

This system of two second-order partial differential equations (PDEs) can be conveniently reduced to a unique fourth-order PDE. The interested reader can find all relevant details in the companion paper [23]; here for conciseness' sake only the essential results will be presented. Indeed from Eq. (2) it follows

$$\frac{\partial \phi}{\partial x} = \frac{\rho}{G\kappa} \frac{\partial^2 v}{\partial t^2} - \frac{\partial^2 v}{\partial x^2}, \tag{4}$$

and by proper use of multivariate differential calculus, $\phi$ can be eliminated in Eq. (3). The resulting fourth-order PDE in terms of $v$ alone is

$$EI \frac{\partial^4 v}{\partial x^4} - \rho I \left(1 + \frac{E}{G\kappa}\right) \frac{\partial^4 v}{\partial t^2 \partial x^2} + \rho A \frac{\partial^2 v}{\partial t^2} + \frac{\rho^2 I}{G\kappa} \frac{\partial^4 v}{\partial t^4} = 0, \tag{5}$$

which is the equation, first established by Timoshenko [86] in 1921, when he was developing a new beam theory able to deal with both shear strain and rotary inertia. Similarly, if $v$ is eliminated in Eq. (3), a fully-decoupled fourth-order PDE in terms of $\phi$ alone is obtained

$$EI \frac{\partial^4 \phi}{\partial x^4} - \rho I \left(1 + \frac{E}{G\kappa}\right) \frac{\partial^4 \phi}{\partial t^2 \partial x^2} + \rho A \frac{\partial^2 \phi}{\partial t^2} + \frac{\rho^2 I}{G\kappa} \frac{\partial^4 \phi}{\partial t^4} = 0. \tag{6}$$

### 2.1 Solutions of the equations of motion

Solutions to Eqs. (5)–(6) are sought such that independent variables, *viz.* $x$ and $t$, are separated. In particular it is assumed that time-dependence is of an harmonic kind, so that free vibrations are possible. Thus one finds

$$v(x, t) = V(x) \exp(\mathrm{i}\omega t), \qquad \phi(x, t) = \Phi(x) \exp(\mathrm{i}\omega t), \tag{7}$$

where $\mathrm{i} = \sqrt{-1}$ is the imaginary unit; then, if primes are used to denote derivatives with respect to $x$, it follows from Eq. (5) (similar expressions follow from Eq. (6), too)

$$V'''' + \frac{\rho \omega^2}{E} \left(1 + \frac{E}{G\kappa}\right) V'' + \frac{\rho \omega^2}{E} \left(\frac{\rho \omega^2}{G\kappa} - \frac{A}{I}\right) V = 0. \tag{8}$$

This is a fourth-order ODE with constant coefficients, whose solutions are to be found in the form of exponential functions $V(x) = \exp(\lambda^\star x)$, where, in general, $\lambda^\star \in \mathbb{C}$.

In particular, the *characteristic equation* associated to Eq. (8) is

$$\lambda^{\star 4} + \frac{\rho \omega^2}{E} \left(1 + \frac{E}{G\kappa}\right) \lambda^{\star 2} + \frac{\rho \omega^2}{E} \left(\frac{\rho \omega^2}{G\kappa} - \frac{A}{I}\right) = 0, \tag{9}$$

*i.e.* a biquadratic algebraic equation, whose independent variable is $\lambda^\star$. The squared roots of Eq. (9) are therefore

$$\lambda_1^{\star 2} = -\frac{\rho\omega^2}{2E}\left(1 + \frac{E}{G\kappa}\right) + \sqrt{\frac{\rho^2\omega^4}{4E^2}\left(1 - \frac{E}{G\kappa}\right)^2 + \frac{\rho\,\omega^2 A}{EI}}, \tag{10}$$

$$\lambda_2^{\star 2} = -\frac{\rho\omega^2}{2E}\left(1 + \frac{E}{G\kappa}\right) - \sqrt{\frac{\rho^2\omega^4}{4E^2}\left(1 - \frac{E}{G\kappa}\right)^2 + \frac{\rho\,\omega^2 A}{EI}}. \tag{11}$$

### 2.2   Analysis of the eigensolutions

While in Eq. (11) it is always $\lambda_2^{\star 2} < 0$, the sign of the other root, $\lambda_1^{\star 2}$, given by Eq. (10) depends on the value of $\omega^2$; there is a special value of $\omega^2$, which correspond to a *transition frequency*,

$$\tilde{\omega}^2 = \frac{G\kappa A}{\rho I}, \tag{12}$$

such that the value of $\lambda_1^{\star 2}$ changes from positive to negative. As a consequence, when solving Eq. (9), the following three cases must be distinguished.

**Case 1.** $\omega^2 < \tilde{\omega}^2$.

For this range of angular frequency, it results: $\lambda_1^{\star 2} > 0$ and $\lambda_2^{\star 2} < 0$. Hence, Eq. (9), has *two real roots*, namely $\pm\sqrt{\lambda_1^{\star 2}}$, and *two purely imaginary conjugate roots*, *viz.* $\pm\mathrm{i}\sqrt{-\lambda_2^{\star 2}}$.

**Case 2.** $\omega^2 = \tilde{\omega}^2$.

In the present case, it follows: $\lambda_1^{\star 2} = 0$ and $\lambda_2^{\star 2} < 0$. In particular,

$$\lambda_2^{\star 2}|_{\omega^2 = \tilde{\omega}^2} = -\tilde{\lambda}_2^2, \tag{13}$$

with

$$\tilde{\lambda}_2 = \sqrt{\frac{A}{I}\left(1 + \frac{G\kappa}{E}\right)} > 0. \tag{14}$$

Consequently there is *a null real root, whose multiplicity is two*, and *one couple of imaginary conjugate roots*, namely again $\pm\mathrm{i}\sqrt{-\lambda_2^{\star 2}}$.

**Case 3.** $\omega^2 > \tilde{\omega}^2$.

This time it results $\lambda_1^{\star 2} < 0$ and $\lambda_2^{\star 2} < 0$.

As a consequence, *all four roots* of Eq. (9) *are purely imaginary*. In particular, there are *two couples of conjugate roots*, *i.e.* $\pm\mathrm{i}\sqrt{-\lambda_1^{\star 2}}$ and $\pm\mathrm{i}\sqrt{-\lambda_2^{\star 2}}$.

### 2.3   The eigenmodes of Timoshenko beams

The complete solution to Eq. (8) and the corresponding equation which provides $\Phi(x)$ can be computed in terms of real-valued quantities only; results will be presented separately for the three cases outlined above. The relevant details are still given in [23].

**Case 1.** $\omega^2 < \tilde{\omega}^2$.

The eigenfunctions in terms of $V(x)$ and $\Phi(x)$ are

$$V(x) = A_1 \cosh \hat{\lambda}_1 x + A_2 \sinh \hat{\lambda}_1 x + A_3 \cos \lambda_2 x + A_4 \sin \lambda_2 x, \tag{15}$$

$$\Phi(x) = -\frac{\hat{\alpha}_1}{\hat{\lambda}_1}(A_2 \cosh \hat{\lambda}_1 x + A_1 \sinh \hat{\lambda}_1 x) + \frac{\alpha_2}{\lambda_2}(A_4 \cos \lambda_2 x - A_3 \sin \lambda_2 x). \tag{16}$$

where the following *proper* ($\lambda_2$) and *generalized* ($\hat{\lambda}_1$) real-valued wave-numbers apply

$$\hat{\lambda}_1 = +\sqrt{\lambda_1^{\star 2}} > 0, \qquad \lambda_2 = +\sqrt{-\lambda_2^{\star 2}} > 0. \tag{17}$$

In Eq. (16) the following short-hand notation has been adopted

$$\hat{\alpha}_1 = \frac{\rho \omega^2}{G\kappa} + \hat{\lambda}_1^2, \qquad \alpha_2 = \frac{\rho \omega^2}{G\kappa} - \lambda_2^2. \tag{18}$$

**Case 2.** $\omega^2 = \tilde{\omega}^2$.

The eigenfunctions have, in this case, these expressions

$$V(x) = C_1 + C_3 \cos \tilde{\lambda}_2 x + C_4 \sin \tilde{\lambda}_2 x, \tag{19}$$

$$\Phi(x) = D_1 - \tilde{\omega}^2 \frac{\rho}{G\kappa} C_1 x - \frac{\tilde{\alpha}_2}{\tilde{\lambda}_2}(C_3 \sin \tilde{\lambda}_2 x - C_4 \cos \tilde{\lambda}_2 x), \tag{20}$$

where, for the seek of a compact notation, the following definition has been adopted, see Eq. (14)

$$\tilde{\alpha}_2 = \frac{\rho \tilde{\omega}^2}{G\kappa} - \tilde{\lambda}_2^2 = -\frac{G\kappa A}{EI}. \tag{21}$$

**Case 3.** $\omega^2 > \tilde{\omega}^2$.

In this last case the eigenfunctions are

$$V(x) = E_1 \cos \lambda_1 x + E_2 \sin \lambda_1 x + E_3 \cos \lambda_2 x + E_4 \sin \lambda_2 x, \tag{22}$$

$$\Phi(x) = \frac{\alpha_1}{\lambda_1}(E_2 \cos \lambda_1 x - E_1 \sin \lambda_1 x) + \frac{\alpha_2}{\lambda_2}(E_4 \cos \lambda_2 x - E_3 \sin \lambda_2 x), \tag{23}$$

where the two independent, real-valued wave-numbers are given by

$$\lambda_1 = +\sqrt{-\lambda_1^{\star 2}}, \qquad \lambda_2 = +\sqrt{-\lambda_2^{\star 2}}. \tag{24}$$

and the following short-hand notation has been adopted

$$\alpha_1 = \frac{\rho \omega^2}{G\kappa} - \lambda_1^2, \tag{25}$$

while $\alpha_2$ is still defined by Eq. $(18)_2$.

## 3   Modal analysis of Timoshenko beams

The results of Section 2 show that the complete spectrum consists of two portions, none of which can be disregarded.

In the first part of the spectrum, which is relevant to natural frequencies $\omega_n < \tilde{\omega}$, the eigenmodes are given, in general, by a linear combination of hyperbolic and trigonometric functions, see Eqs. (15) and (16). Only for particular choices of boundary conditions (BCs) it is possible to annihilate the contribution of hyperbolic functions: this happens, for instance, in the case of a simply-supported beam.

In the second part of the spectrum, corresponding to natural frequencies $\omega_n > \tilde{\omega}$, modal shapes are instead given by a linear combination of trigonometric functions depending on *two different* wave-numbers, $\lambda_1$ and $\lambda_2$, as Eqs. (22) and (23) show. In general, each of these eigenmodes involves *both $\lambda_1$ and $\lambda_2$*, since wave-numbers are entwined (or even entangled); only for particular cases, *e.g.* the simply-supported beam, the contributions of wave-numbers become decoupled.

Moreover, even the transition frequency, $\tilde{\omega}$, might belong to the spectrum, and hence this condition has to be taken into account, too. If the transition frequency is part of the spectrum, modal shapes are given by a linear combination of trigonometric functions depending on just one wave-number, $\tilde{\lambda}_2$ and of a constant function (for $V$), see Eq. (19), or a linear combination of trigonometric functions and a complete linear polynomial (for $\Phi$), as Eq. (20) shows.

In any case, the particular blending of the above-mentioned functions, which provides the actual eigenmode, depends on the applied BCs.

For a single span beam, as long as only transversal vibrations are envisaged, four basic end constraints might be encountered: clamped (or fixed: $V = 0$ and $\Phi = 0$), free ($T = 0$ and $M = 0$), guided ($T = 0$ and $\Phi = 0$), supported (or hinged: $V = 0$ and $M = 0$). With these four basic constraints it is possible to devise ten different combinations of single-span constrained beams, provided that combinations where the constraints are simply reversed (*e.g.* C-F and F-G) are counted only once. These are: clamped-clamped (or *doubly clamped*, C-C), clamped-free (C-F), clamped-guided (C-G), clamped-supported (C-S); free-free (F-F), free-guided (F-G), free-supported (F-S); guided-guided (G-G), guided-supported (G-S); supported-supported (or *simply-supported*, S-S).

For the sake of simplicity the spectrum has been explicitly computed only for two cases, namely the simply-supported (S-S) beam, and the doubly clamped one (C-C), which are somehow representative of all cases which can occur.

### 3.1   Material and geometric data

The case which has been analyzed is the following: a straight uniform and homogeneous beam, whose length is $L = 2$ m, having a square cross-section with side length (either depth or width) $B = 0.1$ m; as a consequence, the cross-section area and area moment of inertia are respectively $A = B^2 = 0.01$ m$^2$; $I = B^4/12 = 1/120,000$ m$^4$. Moreover, the length-to-depth ratio (a rough measure of slenderness) is, in this case, $L/B = 20$.

Material density is assumed to be $\rho = 8000$ kg/m$^3$, Young's modulus $E = 260$ GPa, Poisson's ratio $\nu = 0.3$ so that, under the hypothesis of elastic isotropy, the shear modulus is $G = 100$ GPa. Finally for the shear correction factor the standard value $\kappa = 5/6$ has been adopted, which is suitable for static analysis of a rectangular cross-section.

### 3.2   The case of a simply-supported beam

For such a beam, whose length is $L$, the boundary conditions require that

$$@x = 0 : \quad V = 0 \text{ and } M = 0; \qquad @x = L : \quad V = 0 \text{ and } M = 0. \tag{26}$$

By virtue of Eq. (1)$_2$ the homogeneous condition $M(x) = 0$ is equivalent to imposing $\Phi'(x) = 0$. It follows then

1. for $\omega^2 < \tilde{\omega}^2$

$$\Phi'(x) = -\hat{\alpha}_1(A_1 \cosh \hat{\lambda}_1 x + A_2 \sinh \hat{\lambda}_1 x) - \alpha_2(A_3 \cos \lambda_2 x + A_4 \sin \lambda_2 x). \tag{27}$$

2. for $\omega^2 = \tilde{\omega}^2$

$$\Phi'(x) = -\tilde{\omega}^2 \frac{\rho}{G\kappa} C_1 - \tilde{\alpha}_2(C_3 \cos \tilde{\lambda}_2 x + C_4 \sin \tilde{\lambda}_2 x). \tag{28}$$

154     3. for $\omega^2 > \tilde{\omega}^2$

$$\Phi'(x) = -\alpha_1(E_1 \cos \lambda_1 x + E_2 \sin \lambda_1 x) - \alpha_2(E_3 \cos \lambda_2 x + E_4 \sin \lambda_2 x). \tag{29}$$

155 In what follows, the two parts of the spectrum and the transition frequency will be treated separately.

### 156     3.2.1    First part of the spectrum: $\omega^2 < \tilde{\omega}^2$.

157 When BCs are substituted into Eqs. (15) and (27), the following homogeneous system of simultaneous linear algebraic
158 equations is obtained

$$\mathbf{AX} = \mathbf{0}, \tag{30}$$

159 where the square matrix $\mathbf{A}$ and the column vectors $\mathbf{X}$ and $\mathbf{0}$ have these expressions

$$\mathbf{A} = \begin{bmatrix} 1 & 0 & 1 & 0 \\ \hat{\alpha}_1 & 0 & \alpha_2 & 0 \\ \cosh \hat{\lambda}_1 L & \sinh \hat{\lambda}_1 L & \cos \lambda_2 L & \sin \lambda_2 L \\ \hat{\alpha}_1 \cosh \hat{\lambda}_1 L & \hat{\alpha}_1 \sinh \hat{\lambda}_1 L & \alpha_2 \cos \lambda_2 L & \alpha_2 \sin \lambda_2 L \end{bmatrix}, \quad \mathbf{X} = \begin{Bmatrix} A_1 \\ A_2 \\ A_3 \\ A_4 \end{Bmatrix}, \quad \mathbf{0} = \begin{Bmatrix} 0 \\ 0 \\ 0 \\ 0 \end{Bmatrix}. \tag{31}$$

160 Non-trivial solutions to this matrix problem exist, when the following transcendental equation is satisfied

$$\sinh \hat{\lambda}_1 L \sin \lambda_2 L = 0. \tag{32}$$

161 Disregarding the value $\hat{\lambda}_1 L = 0$ (the only one which annihilates $\sinh \hat{\lambda}_1 L$), it must be

$$\lambda_2 L = k_2 \pi, \quad (k_2 \in \mathbb{N}). \tag{33}$$

162 This gives, for $L \neq 0$, $\lambda_2 = k_2 \pi / L$, and yields, when $k = k_2$, the following *frequency equation* for the simply-supported
163 Timoshenko beam

$$\omega^4 - \frac{G\kappa}{\rho}\left[\frac{A}{I} + \left(\frac{k\pi}{L}\right)^2 \left(1 + \frac{E}{G\kappa}\right)\right]\omega^2 + \frac{EG\kappa}{\rho^2}\left(\frac{k\pi}{L}\right)^4 = 0. \tag{34}$$

164 This Eq. (34) was obtained for the first time in [86], and is again a biquadratic one, whose discriminant, $\Delta^\star$, can be written
165 as

$$\Delta^\star = \left(\frac{G\kappa}{\rho}\right)^2 \left[\left(\frac{A}{I}\right)^2 + 2\frac{A}{I}\left(1 + \frac{E}{G\kappa}\right)\left(\frac{k\pi}{L}\right)^2 + \left(1 - \frac{E}{G\kappa}\right)^2\left(\frac{k\pi}{L}\right)^4\right]. \tag{35}$$

166 Then, the squared solutions to the frequency equation are

$$\omega_1^2 = \frac{1}{2}\left\{\frac{G\kappa}{\rho}\left[\frac{A}{I} + \left(\frac{k\pi}{L}\right)^2\left(1 + \frac{E}{G\kappa}\right)\right] + \sqrt{\Delta^\star}\right\}, \tag{36}$$

$$\omega_2^2 = \frac{1}{2}\left\{\frac{G\kappa}{\rho}\left[\frac{A}{I} + \left(\frac{k\pi}{L}\right)^2\left(1 + \frac{E}{G\kappa}\right)\right] - \sqrt{\Delta^\star}\right\}, \tag{37}$$

167 In the first part of the spectrum, the frequency of vibration corresponding to the $n$-th mode, $\omega_n$, must also comply with
168 these restrictions

$$\omega_n < \tilde{\omega} \quad \text{and} \quad \omega_n < \omega^\star_{k_2}, \tag{38}$$

where the upper bound $\omega^\star_{k_2}$ on the value of $\omega_n$, corresponding to a given value of index $k = k_2$,

$$\omega^\star_{k_2} = \sqrt{\frac{2E}{\rho}\frac{G\kappa}{G\kappa + E}}\left(\frac{k\pi}{L}\right), \tag{39}$$

descends from the requirement that the root (37) of Eq. (34) is strictly positive. So, the only *admissible solutions* are of this kind

$$\omega_n = \omega_{k_2} = +\sqrt{\omega_2^2(k_2)}, \quad (k_2 = 1, \dots, k_2^\star), \quad k_2^\star = \max\{k_2 \in \mathbb{N} \,|\, \omega_{k_2} < \tilde{\omega}\}. \tag{40}$$

The meaning of Eq. (40) is that the $k_2$-th frequency is given by the positive root of Eq. (37) once the value $k_2\pi/L$ has been plugged into Eq. (34).

Thus the natural frequencies for the first part of the spectrum are completely identified; the corresponding eigenmodes, $V_n(x) = V_{k_2}(x)$, $\Phi_n(x) = \Phi_{k_2}(x)$ follow immediately; by assuming, for instance, $A_{4n} = 1$, one finds

$$V_{k_2}(x) = \sin\lambda_2 x; \qquad \Phi_{k_2}(x) = \frac{\alpha_2}{\lambda_2}\cos\lambda_2 x, \tag{41}$$

where integer index $k_2$ belongs to this range: $k_2 = 1, \dots, k_2^\star$. In Eq. (41) $\lambda_2 = \lambda_2(\omega_{k_2})$ and $\alpha_2 = \alpha_2(\omega_{k_2})$ *i.e.* they assume the values corresponding to $\omega_{k_2}$.

### 3.2.2  Transition frequency: $\omega^2 = \tilde{\omega}^2$.

When BCs are substituted into Eqs. (19) and (28), a new homogeneous system of simultaneous linear algebraic equations similar to Eq. (30) is obtained, but in this case the square matrix $\mathbf{A}$ and the column matrix $\mathbf{X}$ are given by

$$\mathbf{A} = \begin{bmatrix} 1 & 1 & 0 & 0 \\ \dfrac{\rho\tilde{\omega}^2}{G\kappa} & \tilde{\alpha}_2 & 0 & 0 \\ 1 & \cos\tilde{\lambda}_2 L & \sin\tilde{\lambda}_2 L & 0 \\ \dfrac{\rho\tilde{\omega}^2}{G\kappa} & \tilde{\alpha}_2\cos\tilde{\lambda}_2 L & \tilde{\alpha}_2\sin\tilde{\lambda}_2 L & 0 \end{bmatrix}, \quad \mathbf{X} = \left\{\begin{array}{c} C_1 \\ C_3 \\ C_4 \\ D_1 \end{array}\right\}, \tag{42}$$

where $\tilde{\lambda}_2$ and $\tilde{\alpha}_2$ are given by Eqs. (14) and (21). The coefficient matrix $\mathbf{A}$ appearing in Eq. (42) has never rank$(\mathbf{A}) > 3$: the homogeneous system of equations is defective, and this is clearly seen, since it does not depend on coefficient $D_1$.

Therefore, when $\sin\tilde{\lambda}_2 L \neq 0$, the above-mentioned matrix has precisely rank$(\mathbf{A}) = 3$, and the only non-trivial solutions are given by $C_1 = C_3 = C_4 = 0$ and $D_1 = D_{1\tilde{\omega}} \neq 0$; in particular the eigenfunction can be normalized so that $D_{1\tilde{\omega}} = 1$.

The eigenfunctions at the transition frequency, *i.e.* when $\omega = \tilde{\omega}$, are hence

$$V_{\tilde{\omega}}(x) = 0, \qquad \Phi_{\tilde{\omega}}(x) = 1. \tag{43}$$

The mode described by Eq. (43) consists of a *pure-shear* vibration mode, where transversal displacement is always zero, while section rotation assumes a constant value, which is the same for all cross-sections: this ensures that flexural effects do not enter into the play.

### 3.2.3  Second part of the spectrum: $\omega^2 > \tilde{\omega}^2$.

In this case, substitution of the BCs into Eqs. (22) and (29), gives a homogeneous system of simultaneous linear algebraic equations which is analogous to Eq. (30), but this time with $\mathbf{A}$ and $\mathbf{X}$ given by

$$\mathbf{A} = \begin{bmatrix} 1 & 0 & 1 & 0 \\ \alpha_1 & 0 & \alpha_2 & 0 \\ \cos \lambda_1 L & \sin \lambda_1 L & \cos \lambda_2 L & \sin \lambda_2 L \\ \alpha_1 \cos \lambda_1 L & \alpha_1 \sin \lambda_1 L & \alpha_2 \cos \lambda_2 L & \alpha_2 \sin \lambda_2 L \end{bmatrix}, \quad \mathbf{X} = \left\{ \begin{array}{c} E_1 \\ E_2 \\ E_3 \\ E_4 \end{array} \right\}. \tag{44}$$

Non-trivial solutions exist, when the following transcendental equation is satisfied

$$\sin \lambda_1 L \sin \lambda_2 L = 0. \tag{45}$$

In order to satisfy Eq.(45), it must be

$$\lambda_1 L = k_1 \pi \quad \text{or} \quad \lambda_2 L = k_2 \pi, \quad (k_1, k_2 \in \mathbb{N}). \tag{46}$$

The former occurrence implies

$$\lambda_1 = k_1 \frac{\pi}{L},$$

which can be satisfied by an infinite sequence of integer indices, $k_1 \in \mathbb{N}$. When searching for admissible solutions for $\lambda_1$, one is faced again with the frequency equation for the simply-supported beam, see Eq. (34). But in this second part of the spectrum, the frequency of vibration must comply with these restrictions

$$\omega_n > \tilde{\omega} \quad \text{and} \quad \omega_n > \omega_{k_1}^\star, \tag{47}$$

where the lower bound $\omega_{k_1}^\star$ on the value of $\omega_n$ (corresponding to a given value of index $k = k_1$),

$$\omega_{k_1}^\star = \sqrt{\frac{2E}{\rho} \frac{G\kappa}{G\kappa + E}} \left( \frac{k\pi}{L} \right), \tag{48}$$

descends from the requirement that the root (36) of Eq. (34) is strictly positive. So only solutions of this kind are *admissible*

$$\omega_n = \omega_{k_1} = +\sqrt{\omega_1^2(k_1)}. \tag{49}$$

As in the previous case, the notation employed in Eq. (49) means that the solution in terms of frequency is given by the positive root of $\omega_1^2$, once the value $k_1 \pi / L$ has been plugged into it. In Eq. (49) the integer index $k_1$ takes values inside this range

$$k_1 = 1, \dots, \infty. \tag{50}$$

By virtue of (49) the natural frequency for this first contribution to the *second part* of the spectrum are completely identified; the corresponding eigenmodes, by assuming $E_{2n} = 1$, are

$$V_{k_1}(x) = \sin \lambda_1 x, \qquad \Phi_{k_1}(x) = \frac{\alpha_1}{\lambda_1} \cos \lambda_1 x, \tag{51}$$

where index $k_1$ takes the values defined by the range (50), while in Eq. (51) $\lambda_1 = \lambda_1(\omega_{k_1})$ and $\alpha_1 = \alpha_1(\omega_{k_1})$, *i.e.* they assume the values corresponding to $\omega_{k_1}$.

The latter occurrence (see Eq. (46)) gives

$$\lambda_2 = k_2 \frac{\pi}{L},$$

and provides, see *e.g.* Eq. (37), the *same* solution already discussed in Section 3.2.1

$$\omega_n = \omega_{k_2} = +\sqrt{\omega_2^2(k_2)}, \quad (k_2 = k_2^\star + 1, \ldots, \infty), \tag{52}$$

with the only remarkable difference that, being now $\omega > \tilde{\omega}$, index $k_2$ must take values in a range which extends beyond the value $k_2^\star$ which has been defined in Eq. (40)$_2$. On the other hand, the same upper bound for $\omega_{k_2}$ represented by Eq. (39) has still to be satisfied: indeed, if it is violated, the root given by Eq. (37) becomes negative.

As a consequence, if the same normalization is assumed, *e.g.* $E_{4n} = 1$, the relevant eigenmodes, provided that index $k_2$ is in the suitable range defined by Eq. (52), are

$$V_{k_2}(x) = \sin \lambda_2 x, \qquad \Phi_{k_2}(x) = \frac{\alpha_2}{\lambda_2} \cos \lambda_2 x, \tag{53}$$

which still coincide with Eq. (41), holding in the first part of the spectrum. This circumstance occurs only in case of a simply-supported beam: other combinations of BCs never produce eigenmodes having the same shape in the first and in the second part of the spectrum.

### 3.3    The case of a doubly clamped beam

When both ends of the beam, whose length is $L$, are built-in, there are only kinematic type BCs

$$@x = 0 : \quad V = 0 \text{ and } \Phi = 0; \qquad @x = L : \quad V = 0 \text{ and } \Phi = 0. \tag{54}$$

Again, the two parts of the spectrum must be treated separately.

### 3.3.1    First part of the spectrum: $\omega^2 < \tilde{\omega}^2$.

When BCs, Eqs. (54) are substituted into Eqs. (15) and (16), this homogeneous system of simultaneous linear algebraic equations, which is similar to Eq. (30) is obtained, where matrix $\mathbf{A}$ assumes now the expression

$$\mathbf{A} = \begin{bmatrix} 1 & 0 & 1 & 0 \\ 0 & \dfrac{\hat{\alpha}_1}{\hat{\lambda}_1} & 0 & -\dfrac{\alpha_2}{\lambda_2} \\ \cosh \hat{\lambda}_1 L & \sinh \hat{\lambda}_1 L & \cos \lambda_2 L & \sin \lambda_2 L \\ \dfrac{\hat{\alpha}_1}{\hat{\lambda}_1} \sinh \hat{\lambda}_1 L & \dfrac{\hat{\alpha}_1}{\hat{\lambda}_1} \cosh \hat{\lambda}_1 L & \dfrac{\alpha_2}{\lambda_2} \sin \lambda_2 L & -\dfrac{\alpha_2}{\lambda_2} \cos \lambda_2 L \end{bmatrix}. \tag{55}$$

For the existence of non-trivial solutions, the following transcendental equation must be satisfied

$$2(1 - \cosh \hat{\lambda}_1 L \cos \lambda_2 L) + \frac{\hat{\lambda}_1 \lambda_2}{\hat{\alpha}_1 \alpha_2} \left( \frac{\alpha_2^2}{\lambda_2^2} - \frac{\hat{\alpha}_1^2}{\hat{\lambda}_1^2} \right) \sinh \hat{\lambda}_1 L \sin \lambda_2 L = 0. \tag{56}$$

For the doubly clamped beam it is not possible to arrive at a closed-form solution: natural frequencies $\omega_n$ have to be determined by solving Eq. (56) once the expressions of $\hat{\lambda}_1(\omega)$, $\lambda_2(\omega)$, $\hat{\alpha}_1(\omega)$, $\alpha_2(\omega)$ are plugged into it, producing a complicated implicit transcendental equation in $\omega$.

It is necessary, of course, to restrict the search for solutions to the range $0 < \omega_n < \tilde{\omega}$, since only in this range Eq. (56) is guaranteed to assume real values. If the roots of Eq. (56) are then denoted by $\omega_n, (n = 1, \ldots, \tilde{n})$, with

$$\tilde{n} = \max \{ n \in \mathbb{N} \,|\, \omega_n < \tilde{\omega} \}, \tag{57}$$

the corresponding values of $\hat{\lambda}_1, \lambda_2, \hat{\alpha}_1, \alpha_2$ might be usefully denoted by

$$\hat{\lambda}_{1n} = \hat{\lambda}_1(\omega_n), \quad \lambda_{2n} = \lambda_2(\omega_n), \quad \hat{\alpha}_{1n} = \hat{\alpha}_1(\omega_n), \quad \alpha_{2n} = \alpha_2(\omega_n). \tag{58}$$

Then, once a solution $\omega_n$ is found, the corresponding eigenfunctions can be determined. If, for normalizing purposes $A_{4n} = 1$ is assumed, then it follows

$$A_{1n} = -\sigma_n, \quad A_{2n} = \hat{\chi}_n, \quad A_{3n} = \sigma_n, \quad \sigma_n = \frac{\hat{\chi}_n \sinh \hat{\lambda}_{1n} L + \sin \lambda_{2n} L}{\cosh \hat{\lambda}_{1n} L - \cos \lambda_{2n} L}, \quad \hat{\chi}_n = \frac{\alpha_{2n} \hat{\lambda}_{1n}}{\hat{\alpha}_{1n} \lambda_{2n}}. \tag{59}$$

These values allow completing by Eqs (15) and (16) the construction of the eigenmodes. For a doubly clamped beam, the eigenmodes corresponding to the *first part* of the spectrum consist of all four functions $\cosh \hat{\lambda}_{1n} x$, $\sinh \hat{\lambda}_{1n} x$, $\cos \lambda_{2n} x$, $\sin \lambda_{2n} x$.

### 3.3.2 Transition frequency: $\omega^2 = \tilde{\omega}^2$.

When BCs are substituted into Eqs. (19) and (20), a homogeneous system of simultaneous linear algebraic equations similar to Eq. (30) is obtained, where

$$\mathbf{A} = \begin{bmatrix} 1 & 1 & 0 & 0 \\ 0 & 0 & \dfrac{\tilde{\alpha}_2}{\tilde{\lambda}_2} & 1 \\ 1 & \cos \tilde{\lambda}_2 L & \sin \tilde{\lambda}_2 L & 0 \\ -\dfrac{\rho \tilde{\omega}^2}{G\kappa} L & -\dfrac{\tilde{\alpha}_2}{\tilde{\lambda}_2} \sin \tilde{\lambda}_2 L & \dfrac{\tilde{\alpha}_2}{\tilde{\lambda}_2} \cos \tilde{\lambda}_2 L & 1 \end{bmatrix}, \quad \mathbf{X} = \left\{ \begin{array}{c} C_1 \\ C_3 \\ C_4 \\ D_1 \end{array} \right\}. \tag{60}$$

The determinant of the coefficient matrix $\mathbf{A}$ might be simplified and becomes

$$\det(\mathbf{A}) = (1 - \cos \tilde{\lambda}_2 L) - \frac{1}{2\tilde{\alpha}_2} \frac{\rho \tilde{\omega}^2}{G\kappa} \tilde{\lambda}_2 L \sin \tilde{\lambda}_2 L \tag{61}$$

For an assigned value of $L$, Eq. (61) is completely determined and, in general, it is $\det(\mathbf{A}) \neq 0$: this implies that the coefficient matrix is non-singular, so that the only solution to Eq. (30) is the trivial one, namely $C_1 = C_3 = C_4 = D_1 = 0$: as a consequence both $V(x) = 0$ and $\Phi(x) = 0$, and it comes out that (in general) *the transition frequency is not part of the spectrum for the doubly clamped beam*, since at such frequency there are no vibrations.

This situation corresponds to values of the beam length such that it is *impossible* to place a suitable number of sine/cosine waves along the beam span which can, at the same time, satisfy the BCs at both ends of the beam.

### 3.3.3 Second part of the spectrum: $\omega^2 > \tilde{\omega}^2$.

As in the already considered cases, substitution of the BCs into Eqs. (22) and (23), gives a homogeneous system of simultaneous linear algebraic equations analogous to Eq. (30), where in the present case

$$\mathbf{A} = \begin{bmatrix} 1 & 0 & 1 & 0 \\ 0 & \dfrac{\alpha_1}{\lambda_1} & 0 & \dfrac{\alpha_2}{\lambda_2} \\ \cos \lambda_1 L & \sin \lambda_1 L & \cos \lambda_2 L & \sin \lambda_2 L \\ -\dfrac{\alpha_1}{\lambda_1} \sin \lambda_1 L & \dfrac{\alpha_1}{\lambda_1} \cos \lambda_1 L & -\dfrac{\alpha_2}{\lambda_2} \sin \lambda_2 L & \dfrac{\alpha_2}{\lambda_2} \cos \lambda_2 L \end{bmatrix}, \quad \mathbf{X} = \left\{ \begin{array}{c} E_1 \\ E_2 \\ E_3 \\ E_4 \end{array} \right\}. \tag{62}$$

Non-trivial solutions might be shown to exist, provided that the following transcendental equation is satisfied

$$2(1 - \cos \lambda_1 L \cos \lambda_2 L) - \frac{\lambda_1 \lambda_2}{\alpha_1 \alpha_2} \left( \frac{\alpha_1^2}{\lambda_1^2} + \frac{\alpha_2^2}{\lambda_2^2} \right) \sin \lambda_1 L \sin \lambda_2 L = 0. \tag{63}$$

Again, for the doubly clamped beam it is not possible to arrive at a closed form solution: natural frequencies $\omega_n$ have to be determined by solving Eq. (63) once the expressions of $\lambda_1(\omega)$, $\lambda_2(\omega)$, $\alpha_1(\omega)$, $\alpha_2(\omega)$ are plugged into it, producing a complicated implicit transcendental equation in $\omega$.

It is necessary, of course, to restrict the search for solutions to the range $\omega_n > \tilde{\omega}$, since only in this range Eq. (63) is guaranteed to assume real values. If the roots of Eq. (63) are denoted by $\omega_n, (n = \tilde{n} + 1, \ldots, \infty)$, with $\tilde{n}$ defined by Eq. (57), the corresponding values of $\lambda_1, \lambda_2, \alpha_1, \alpha_2$ might be usefully denoted by

$$\lambda_{1n} = \lambda_1(\omega_n), \quad \lambda_{2n} = \lambda_2(\omega_n), \quad \alpha_{1n} = \alpha_1(\omega_n), \quad \alpha_{2n} = \alpha_2(\omega_n). \tag{64}$$

Once a solution $\omega_n$ is found, the corresponding eigenfunctions can be determined. If, for normalizing purposes $E_{4n} = 1$ is assumed, then it follows

$$E_{1n} = -\tau_n, \quad E_{2n} = \chi_n \quad E_{3n} = \tau_n, \quad \tau_n = \frac{\chi_n \sin \lambda_{1n} L + \sin \lambda_{2n} L}{\cos \lambda_{1n} L - \cos \lambda_{2n} L}, \quad \chi_n = -\frac{\alpha_{2n} \lambda_{1n}}{\alpha_{1n} \lambda_{2n}}. \tag{65}$$

This allows completing by Eqs. (22) and (23) the construction of the eigenmodes. For a doubly clamped beam all four functions $\cos \lambda_{1n} x$, $\sin \lambda_{1n} x$, $\cos \lambda_{2n} x$, $\sin \lambda_{2n} x$ appear in the eigenmodes which are relevant to the second part of the spectrum.

## 4    Finite element models of Timoshenko beam

In order to verify the accuracy of the numerical solution in terms of both natural frequencies (the eigenvalues of the dynamic problem) and of the vibration modes (the corresponding eigenvectors) the complete frequency spectrum has been computed for different finite element models. Considering a given number $N$ of DOFs, the complete discretized frequency spectrum consists of $N$ components.

The approach of studying the complete discretized spectrum has been proposed by Hughes [52][pp. 429–455] for the longitudinal vibration of rods and the transversal vibrations of Euler-Bernoulli beams by means of standard Lagrangian finite elements. For these classes of structures, the same study has been performed by Reali [78] using an isogeometric analysis (IGA) approach. As far as the authors know, the complete frequency spectrum for the Timoshenko beam model has not been developed, yet, using finite elements. For this reason, in this paper, four different meshes have been adopted with a Non Uniform Rational Basis Spline (NURBS) approximation, and two other models were built using standard Finite Elements (FEM) with Lagrangian shape function. The nodal variables are in both cases the transversal displacement and the rotation at each control point (for IGA), or at each node, for the standard FEM.

For the Lagrangian finite element models a commercial code has been chosen (see [33]), by adopting linear and quadratic shape functions. In particular the linear ($p = 1$) model was built by means of 2-noded, elements, labeled B21 in the code manual, which take into account both shear strain and rotary inertia. Their shape functions, $L_{11}$ and $L_{21}$, (the first index denotes the node, the second the polynomial order) are the usual linear functions, defined in the parameter space spanned by $\xi \in [-1, 1]$ and depicted in Figure 2(a). The mass matrix associated to them is a *lumped* one.
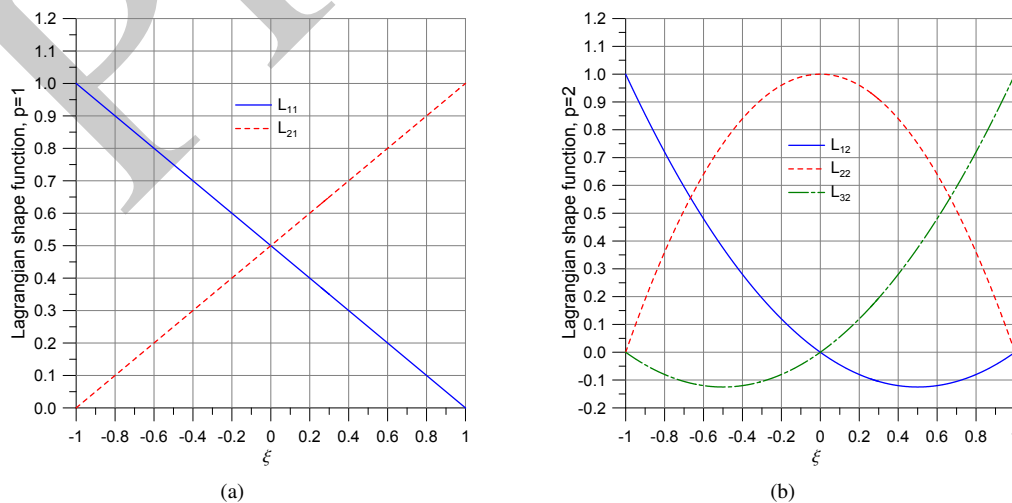


**Fig. 2** Lagrangian shape functions for Timoshenko beam finite elements: linear shape functions (a); parabolic shape functions (b).

278     The quadratic ($p = 2$) model was obtained by means of 3-noded elements, which are also known as `B22`. In this case,
279 shear strain and rotary inertia have been considered, too. Variables are described by means of standard quadratic shape
280 functions ($L_{12}, L_{22}, L_{32}$) which are depicted in Figures 2(b); for this model, however, the mass matrix is a *consistent* one.
281     Stiffness and mass matrices for these elements (`B21` and `B22`) are built by numerical integration adopting 2 Gauss
282 points. The eigenvalue extraction algorithm for these models is the well known Lanczos algorithm [56].
283     For the IGA models, an in house home-made developed code has been adopted, which is based on a popular computer
284 algebra system with extended numerical facilities (*viz.* [61]) and is built above the GeoPDEs package [34]. The same code
285 has been already applied to static problems for curved beams in [20–22, 27].
286     For the sake of conciseness only the basic ingredient of isogeometric analysis are provided here: the interested reader
287 who needs a more detailed description of B-splines and NURBS approximation is referred to Piegl & Tiller's book, [70],
288 while a general introduction to IGA can be found in [30].
289     It can be stated that a curve $\mathbf{x} = \mathbf{x}(\xi)$ has a $p$-degree NURBS representation when there exist $n \in \mathbb{N}$, control points $\mathbf{P}_j \in$
290 $\mathbb{R}^2$, with associated weights $g_j \in \mathbb{R}$, $j = 0 \ldots n$, and a *knot vector*, *i.e.* a set $\Xi = \{0 = \xi_1 \leq \xi_2 \leq \ldots \leq \xi_{n+p+1} = 1\}$
291 such that, for any $\xi \in [0, 1]$ (the standard parameter space for NURBS and B-splines)

$$\mathbf{x}(\xi) = \sum_{j=0}^{n} R_{j,p}(\xi)\,\mathbf{P}_j, \tag{66}$$

292 where the NURBS basis functions $\{R_{j,p}(\xi)\}$ are expressed by

$$R_{j,p}(\xi) = \frac{B_{j,p}(\xi)g_j}{\displaystyle\sum_{j=0}^{n} B_{j,p}(\xi)g_j}\,. \tag{67}$$

293 The most effective analytical expression for these kinds of functions is the Cox-De Boor recursive formula. It defines the
294 B-splines basis $\{B_{j,p}(\xi)\}$ of order $p$, which is required to build the NURBS basis function as follows

$$B_{j,0}(\xi) = \begin{cases} 1 & \text{if} \quad \xi_j \leq \xi < \xi_{j+1} \\ 0 & \text{otherwise} \end{cases}, \tag{68}$$

$$B_{j,p}(\xi) = \frac{\xi - \xi_j}{\xi_{j+p} - \xi_j} B_{j,p-1}(\xi) + \frac{\xi_{j+p+1} - \xi}{\xi_{j+p+1} - \xi_{j+1}} B_{j+1,p-1}(\xi). \tag{69}$$

295 A partition of the parameter space $[0, 1]$ is defined by the knot vector $\Xi$, which is a non-decreasing set of coordinates. It
296 is possible to have *uniform* and *non uniform* knot-vectors. The latter case corresponds to a set of unequally spaced knots,
297 which allow representing a larger number of shapes. Also the *multiplicities* of *knot values* have important effects on the
298 properties of the basis. It is possible, indeed, to modify the continuity of the NURBS by varying this parameter: repeated
299 knots would reduce it.
300     In this paper four isogeometric finite element models were developed for each case. They have different NURBS degree:
301 quadratic ($p = 2$); cubic ($p = 3$); quartic ($p = 4$); and quintic ($p = 5$). These models are characterized by a uniform knot
302 vector and produce a consistent mass matrix. For matrix integration the number of Gauss points is always assumed equal
303 to the NURBS degree. For example, for cubic elements, ($p = 3$), three Gauss points were used. In Figure 3 the B-spline
304 shape functions, which are the building blocks for constructing the NURBS ones, see Eqs. (67)–(69), are plotted for several
305 different values of the degree $p$. It is useful noticing that these basis functions, similarly to the Lagrangian basis functions,
306 constitute a partition of unity, in the sense that for any $\xi$ it results

$$\sum_{k=0}^{p} B_{j,k}(\xi) = 1.$$

307 However, differently from Lagrangian basis functions of order $p > 1$, the B-splines basis functions (and the NURBS ones,
308 too) are always positive, as a careful check of Figures 2–3 confirms.
309     The generalized eigenvalue problem has been solved for the IGA elements by means of the native function `eig`, which
310 is based on the QZ algorithm [63].
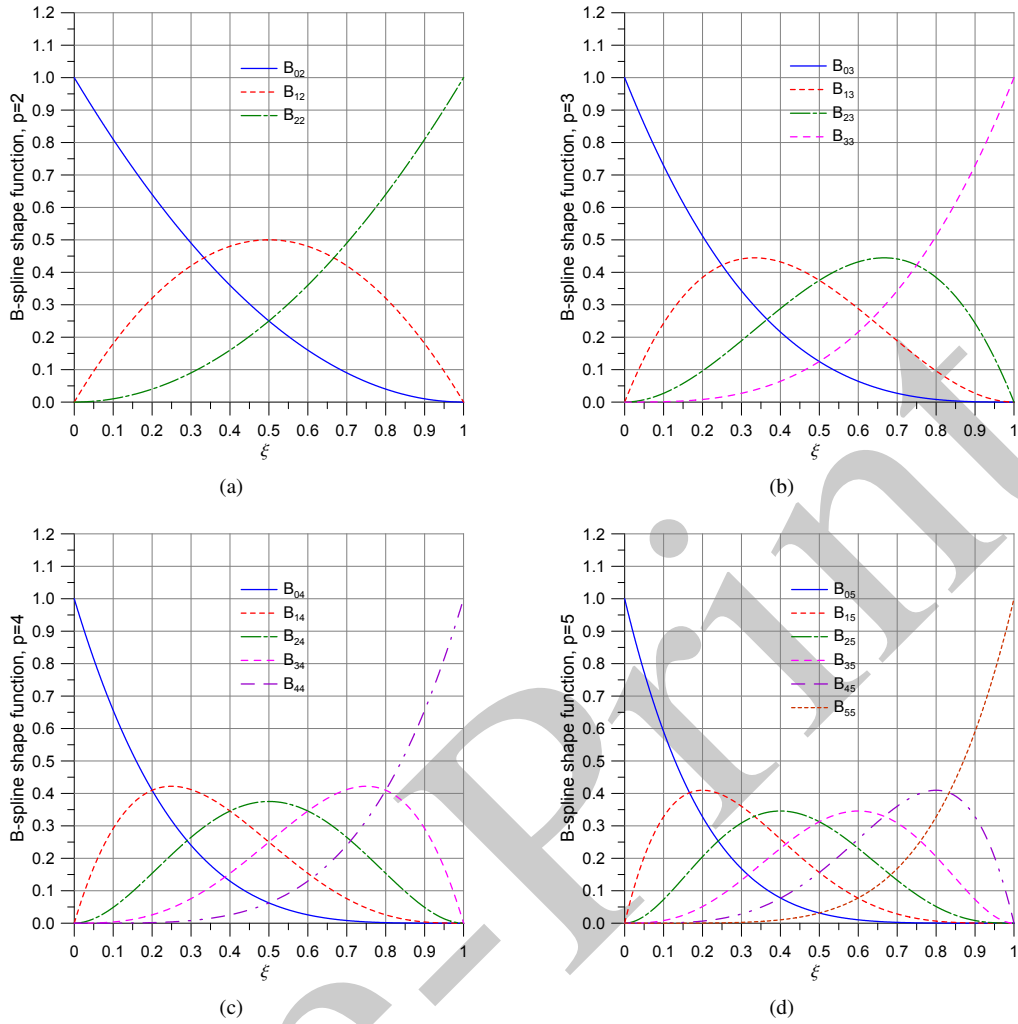
**Fig. 3** B-splines basis function $B_{j,p}$ for Timoshenko beam finite elements and several polynomial order. (a) refers to $p = 2$; (b) to $p = 3$; (c) to $p = 4$; (d) to $p = 5$. The first index refers to the $j$-th control point.

## 5 Computational assessment of Timoshenko beam dynamics

The numerical results presented in this Section aim at assessing the computational performance of the Timoshenko beam model in the simplest dynamic range, corresponding to free vibrations. From the finite element point of view, this corresponds to assembling the mass and stiffness matrices, denoted by $\mathbf{M}$ and $\mathbf{K}$ respectively, and in solving the Generalized (symmetric) Eigenvalue Problem (GEP)

$$(\mathbf{K} - \omega^2 \mathbf{M})\boldsymbol{\Psi} = \mathbf{0}, \tag{70}$$

where $\boldsymbol{\Psi}$ denotes the eigenvector (*i.e.* the *discretized* vibration mode) associated to the natural frequency $\omega$, which holds the place of the eigenvalue.

Once eigenvalues and corresponding eigenvectors are computed for the discretized system, the results are checked against the theoretically *exact* values provided by the solution of the continuum problem which has been presented in Section 3.

In particular, several aspects of the numerical solution have to be addressed: the accuracy of the computed spectrum for the simply-supported and for the doubly clamped beam, the accuracy by which the (discrete) eigenvector reproduces the corresponding eigenmode of the continuous system, and the detection of the last pair (natural frequency $\omega_n$, vibration mode $\boldsymbol{\Psi}_n$) which, for a given number of DOFs, is still sufficiently correct for reproducing the continuous system. These issues are considered separately in the next Sections.

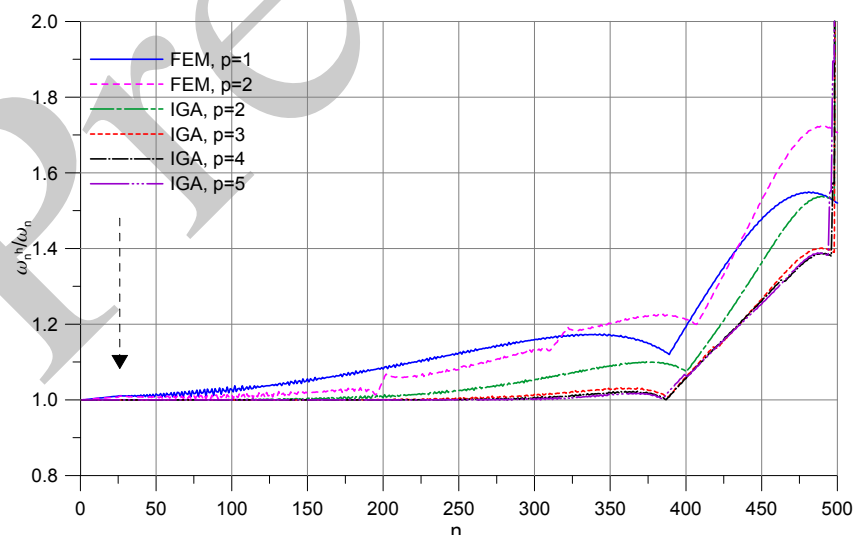### 5.1 Numerical spectrum for a simply-supported Timoshenko beam

The whole frequency spectrum of a simply-supported Timoshenko beam, with the geometric and mechanical characteristics already defined in Section 3.1 has been computed by means of the above mentioned numerical models. The frequency spectra, which are relevant to a total number of DOFs equal to $N = 100$, $N = 500$ and $N = 1000$ have been considered, and are plotted in Figures 4–6.

In each plot, the ratio between the numerical eigenfrequency $\omega_n^h$ and the corresponding analytical one $\omega_n$ is reported on the vertical axis, while the horizontal axis lists natural frequencies in increasing order. Each spectrum is plotted with a different pattern to distinguish the polynomial degree $p$. Moreover, label FEM refers to the Lagrangian models while IGA represents the isogeometric ones. The vertical arrow highlights the position of the cut-off frequency, $\tilde{\omega}$, see Eq. (12).
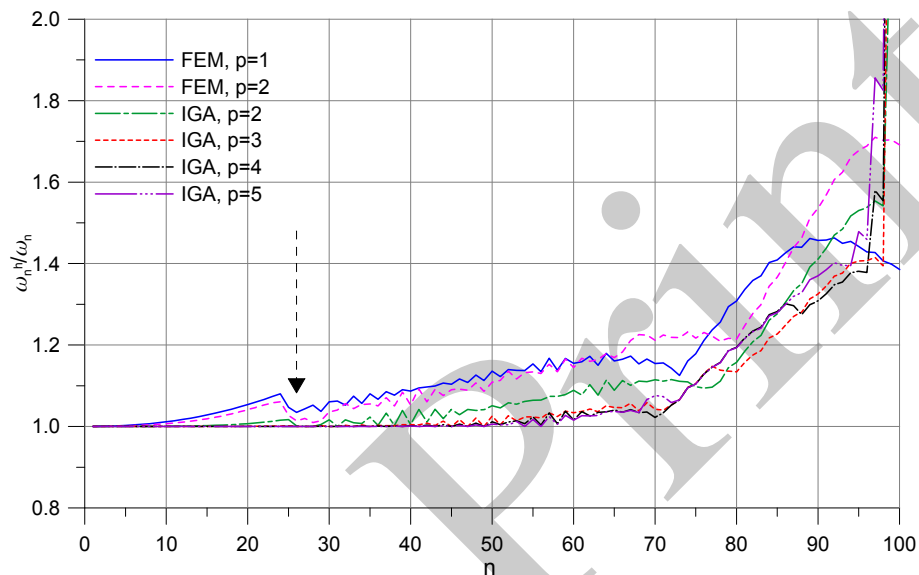


**Fig. 4** Numerical errors of the frequency spectra for a simply-supported Timoshenko beam discretized with $N = 100$ DOFs. The dotted vertical arrow represents the position within the spectrum of the cut-off frequency.



**Fig. 5** Numerical errors of the frequency spectra for a simply-supported Timoshenko beam discretized with $N = 500$ DOFs. The dotted vertical arrow represents the position within the spectrum of the cut-off frequency.

The general trend of these spectra is very similar in all three cases, though, as the number of DOFs increases, curves assume a smoother trend. Roughly speaking, IGA models produce very accurate results for almost 80% of the whole spectrum and exhibit better performances (which, of course, depend on the NURBS degree $p$ and increase with it) in comparison
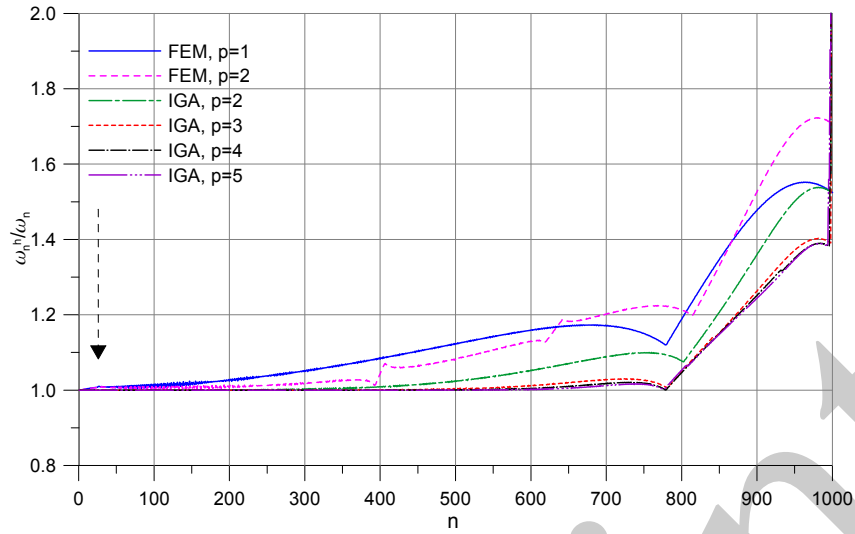
**Fig. 6** Numerical errors of the frequency spectra for a simply-supported Timoshenko beam discretized with $N = 1000$ DOFs.The dotted vertical arrow represents the position within the spectrum of the cut-off frequency.

with the FEM ones, in almost all the spectrum, excluding the very last part of it. Indeed there some *outlier* frequencies appear, which are due to the truncation error produced by the discretization of a continuum problem: these highest frequency samples correspond to highly localized vibration modes (see Figure 7), which show a behavior comparable to a boundary layer.
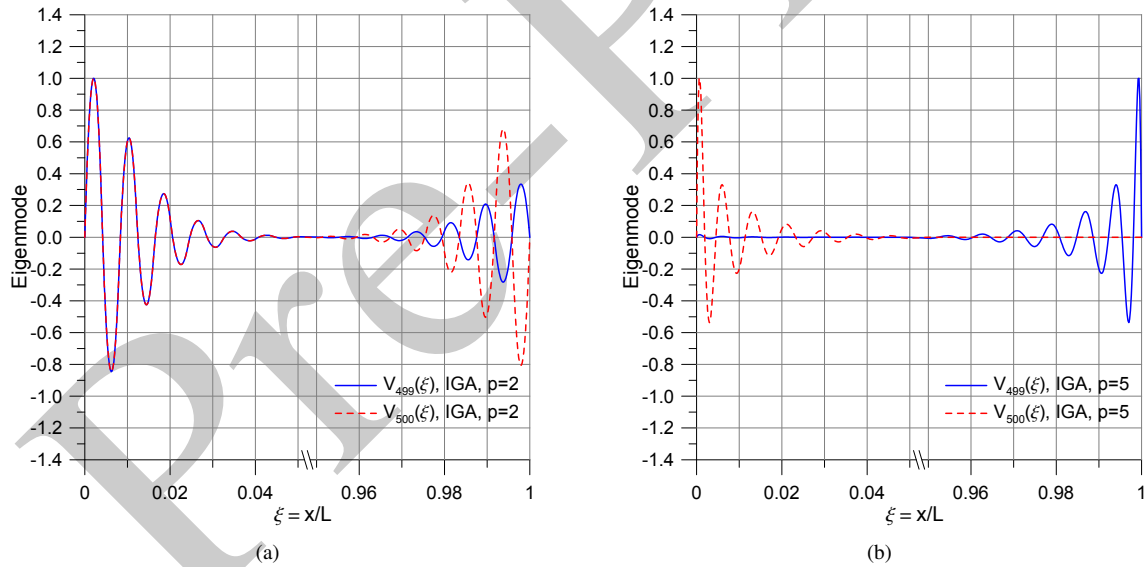


**Fig. 7** Eigenmodes corresponding to *outlier* frequencies, which are typical of IGA elements at the end of the discretized spectrum. In the present case modes 499 and 500 are shown, with reference only to the transversal displacement, $V(x)$. NURBS order: $p = 2$ (a); $p = 5$ (b).

The results of the Lagrangian (FEM) models are quite different in comparison with what happens in the Euler-Bernoulli beam case, whose results can be found in [52], [54]). In that case, indeed, a quite important discontinuity can be detected in the middle of the spectrum, while for the Timoshenko beam the behavior is less jumpy and globally smoother.

## 5.2 Numerical spectrum for a doubly clamped Timoshenko beam

The same analysis has been performed for a doubly clamped Timoshenko beam with the same geometric and mechanical data, too. Only the case $N = 100$ DOFs has been studied, due to the difficulties in computing the exact frequencies, as it has already outlined in Section 3.3.
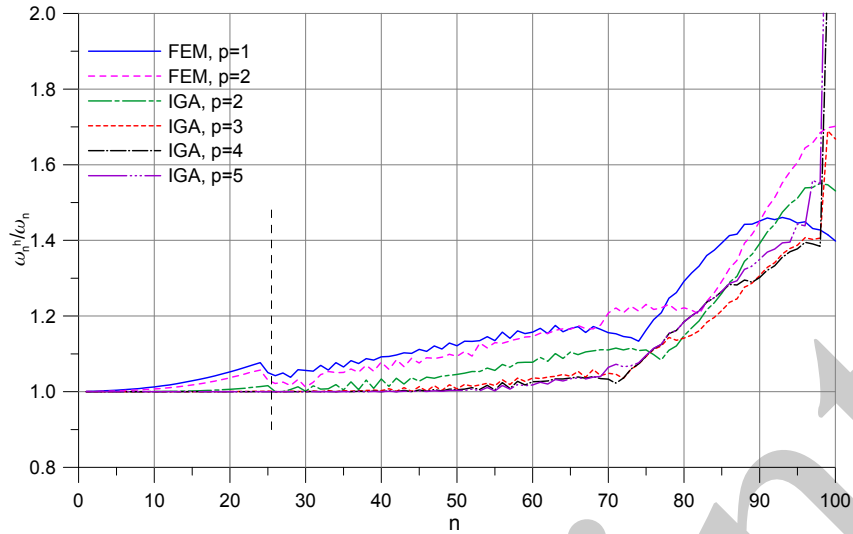
**Fig. 8** Numerical errors of the frequency spectra for a doubly clamped Timoshenko beam discretized with $N = 100$ DOFs. The dotted vertical line represents the boundary between the first and the second part of the spectrum. In this case, the transition frequency $\tilde{\omega}$ *does not* belong to the spectrum.

The eigenfrequency errors are reported in Figure 8: the trend is similar to the simply-supported beam case. Again IGA models produce more accurate results than the standard Lagrangian FEM models.

It is important to highlight that this circumstance proves the reliability and the robustness of the proposed approach, independently of the applied boundary conditions.

### 5.3 Numerical assessment of the quality of the discrete eigenmodes for the Timoshenko beam

The accuracy of the GEP cannot be ascertained by looking only at vibration frequencies, as it has been done, up to now, for the Euler-Bernoulli beam (see [52], [78]). For this reason, an evaluation of the numerically obtained eigenmodes has been performed, for the simply-supported beam only, since in this case the exact eigenmodes are easily computed by Eqs. (41), (43), (51), (53), and, except for the transition frequency, they turn out to be pure sinusoidal functions.

Thus, with the aim of assessing the accuracy of the numerical results, for the simply-supported Timoshenko beam discretized with $N = 500$ DOFs, the whole set of $500$ eigenvectors has been developed: each eigenmode has been reconstructed by evaluating it in $N_p = 5001$ equally spaced points along the beam span; the exact solution has been similarly computed by evaluating in the *same* points the corresponding theoretical eigenmode.

For the sake of conciseness, and to avoid problems related to different normalization criteria, only the transversal displacement component, $V(x)$, has been taken into consideration, but conclusions easily extend to section rotation, $\Phi$, too.

As an accuracy check the $l^2$ discrete relative error (*i.e.* the relative error in the discrete $l^2$ norm) has been computed for each mode: if $V^\star(x)$ denotes the exact eigenmode and $\tilde{V}(x)$ the numerically computed one, it follows

$$l^2 = \frac{\sqrt{\dfrac{1}{N_p} \sum_{j=1}^{N_p} \left[ V^\star(x_j) - \tilde{V}(x_j) \right]^2}}{\sqrt{\dfrac{1}{N_p} \sum_{j=1}^{N_p} \left[ V^\star(x_j) \right]^2}} . \tag{71}$$

Results are plotted in Figures 9–14, separately the two Lagrangian FEM meshes and the four NURBS-based ones.

In order to explain the somehow weird behavior of the $l^2$ error plots, it is useful recalling that, in the *continuum* case, the $L^2$ norm of $\sin j\pi x$ and of $(\sin j\pi x - \sin k\pi x)$ (for $k \neq j$) in the $[0, 1]$ interval are respectively given by
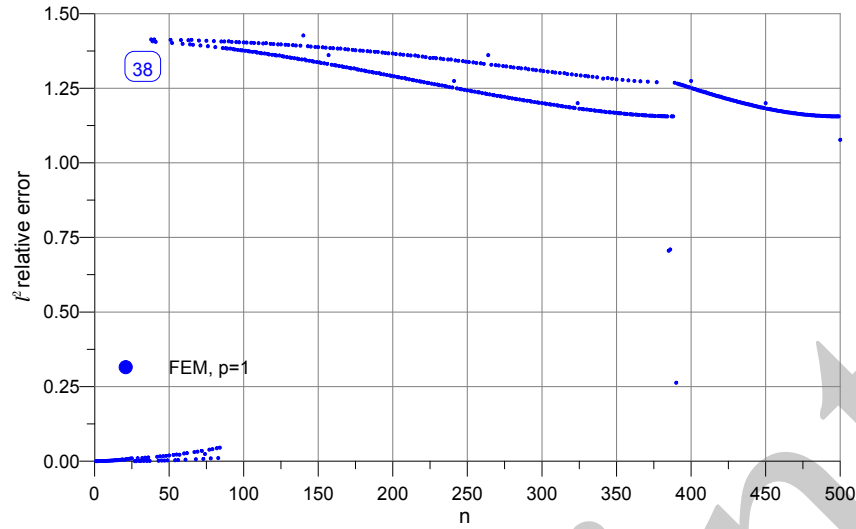
**Fig. 9** $l^2$ norm of the error for the eigenmodes of a simply-supported Timoshenko beam discretized with $N = 500$ DOFs and `B21` linear elements. Each eigenmode has been represented by $N_p = 5001$ equally spaced points along the beam span. The number within the frame represents the first mode affected by non-negligible errors.
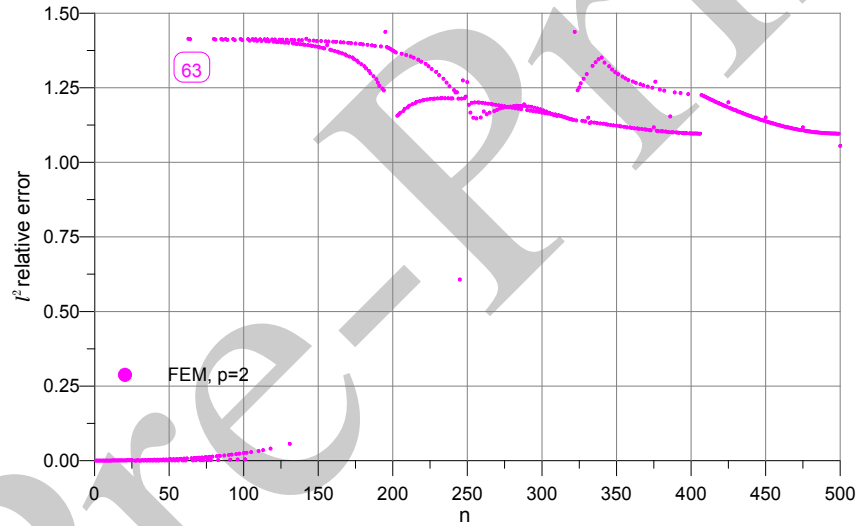


**Fig. 10** $l^2$ norm of the error for the eigenmodes of a simply-supported Timoshenko beam discretized with $N = 500$ DOFs and `B22` quadratic elements. Each eigenmode has been represented by $N_p = 5001$ equally spaced points along the beam span. The number within the frame represents the first mode affected by non-negligible errors.

$$\| \sin j\pi x \|_{L^2} = \left[ \int_0^1 (\sin j\pi x)^2 dx \right]^{1/2} = \frac{1}{\sqrt{2}},$$

$$\|(\sin j\pi x - \sin k\pi x)\|_{L^2} = \left[ \int_0^1 (\sin j\pi x - \sin k\pi x)^2 dx \right]^{1/2} = 1.$$

Consequently, when two different sinusoidal waves are considered, the $L^2$ error is equal to 1, while when the difference between a sinusoidal wave and an almost vanishing function (as it happens for the eigenmodes corresponding to an outlier frequency), then the $L^2$ error becomes equal to $1/\sqrt{2}$. Hence, the error in the $L^2$ norm is higher in the former case than it is in the latter, and this justifies why the observed $l^2$ error tends to reduce at the end of the spectrum.

On the other hand, the very high error values which are found at the beginning of the spectrum correspond to computed eigenmodes which have an incorrect wave-number, as a result of some drift (or aliasing) of the corresponding natural frequencies. This issue will be better illustrated in Section 5.4.

However, looking at Figures 9–14, a faster decay of the quality of solution in terms of eigenmodes is detected in comparison with the accuracy reduction in the frequency range. Indeed Lagrangian elements (see Figures 9–10) exhibit a significant decay after only 38 (linear elements, B21) or 63 (quadratic elements, B22) modes out of 500. Instead, as long as frequencies are concerned, reasonably good results (with error below 20%) were obtained up to mode 300, see Figure 5. If IGA models are considered, their performances are superior even in terms of eigenmode reconstruction: for the quadratic NURBS ($p = 2$), Figure 11, significant decay corresponds to mode 114, while, for the more refined quintic NURBS ($p = 5$, see Figure 14), results are excellent up to mode 271.

In any way, the obtained results clearly show that the quality of approximation of eigenmodes is a crucial points for the Timoshenko beam model, and these plots should be carefully considered before choosing the number, $N$, of DOFs which is necessary to adopt for reproducing, to within a given accuracy, the eigenmode corresponding to a *fixed* natural mode, say the $n$-th.
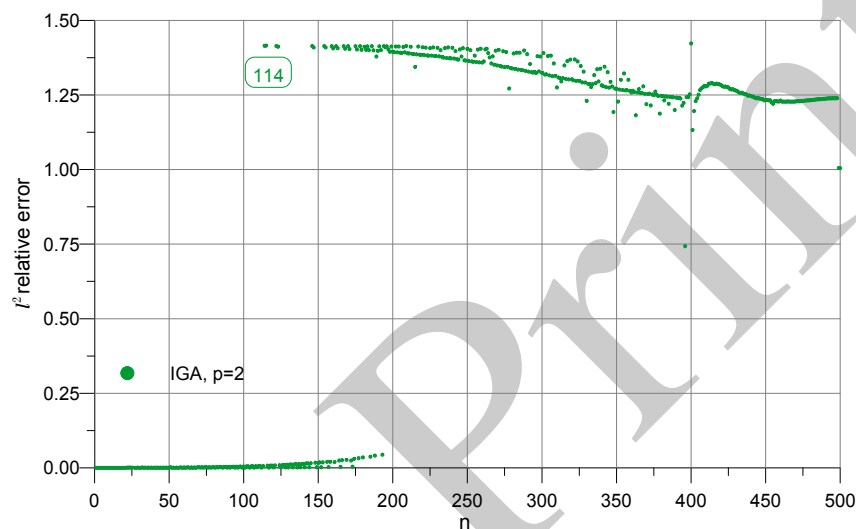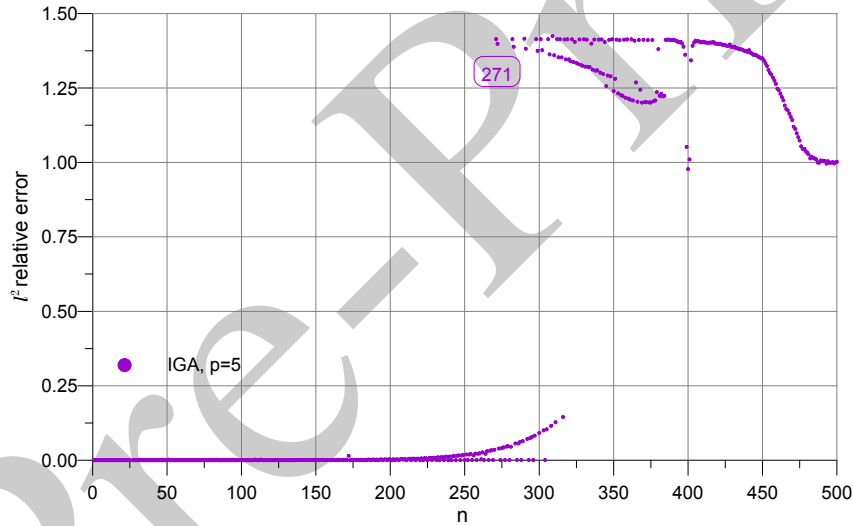


**Fig. 11**  $l^2$ norm of the error for the eigenmodes of a simply-supported Timoshenko beam discretized with $N = 500$ DOFs and IGA elements with $p = 2$. Each eigenmode has been represented by $N_p = 5001$ equally spaced points along the beam span. The number within the frame represents the first mode affected by non-negligible errors.
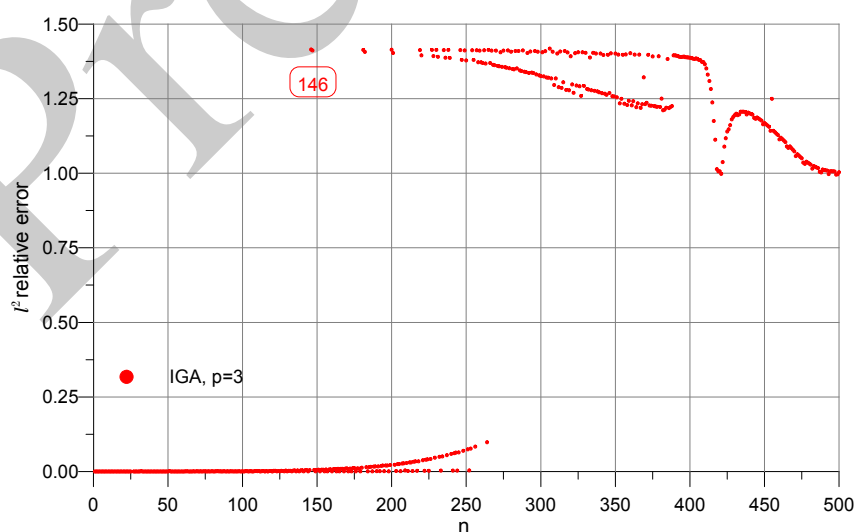


**Fig. 12**  $l^2$ norm of the error for the eigenmodes of a simply-supported Timoshenko beam discretized with $N = 500$ DOFs and IGA elements with $p = 3$. Each eigenmode has been represented by $N_p = 5001$ equally spaced points along the beam span. The number within the frame represents the first mode affected by non-negligible errors.
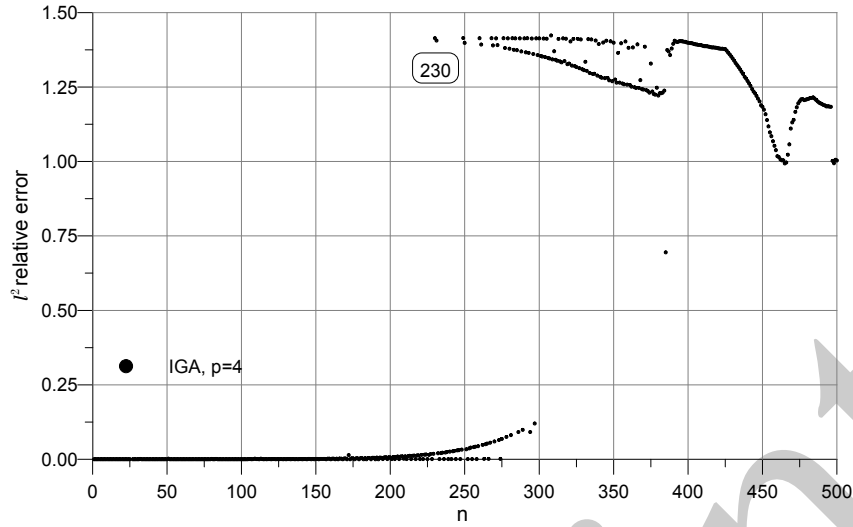
**Fig. 13**   $l^2$ norm of the error for the eigenmodes of a simply-supported Timoshenko beam discretized with $N = 500$ DOFs and IGA elements with $p = 4$. Each eigenmode has been represented by $N_p = 5001$ equally spaced points along the beam span. The number within the frame represents the first mode affected by non-negligible errors.



**Fig. 14**   $l^2$ norm of the error for the eigenmodes of a simply-supported Timoshenko beam discretized with $N = 500$ DOFs and IGA elements with $p = 5$. Each eigenmode has been represented by $N_p = 5001$ equally spaced points along the beam span. The number within the frame represents the first mode affected by non-negligible errors.

### 5.4   Automatic check of the quality of the discrete eigenmodes for the Timoshenko beam

In order to check the accuracy of a numerically computed eigenmode, a simple method would consist in visually inspecting and comparing it against the theoretically exact one. This task, however, is time consuming and becomes more and more inconvenient, when the mode number increases (and the corresponding eigenmode becomes more and more complicated).

For the simply-supported Timoshenko beam, the component $V(x)$ of the eigenmodes, except for that corresponding to the transition frequency, are pure sinusoidal functions, each one depending on a particular wave-number, $\lambda_n$, which descends from either $\lambda_1$ or $\lambda_2$. Therefore, for the $n$-th natural frequency, the relevant eigenmode is given by this *monocromatic* wave

$$V_n(x) = \sin \lambda_n x = \sin \frac{k_n \pi}{L} x, \quad (k_n = k_1 \text{ or } k_n = k_2). \tag{72}$$

In Eq. (72) the wave-number $\lambda_n = k_n\pi/L$ can be thought of as the counterpart of the angular frequency $\omega$ in the time response; analogously, the counterpart of the time frequency $f = \omega/(2\pi)$ in the space domain is the so-called *space-frequency*, $f_{\lambda n}$

$$f_{\lambda n} = \frac{\lambda_n}{2\pi} = \frac{k_n}{2L}. \tag{73}$$

This space-frequency (which corresponds to the *number of complete sinusoidal waves included in the full span $L$ of the beam*), completely characterizes the sinusoidal wave: indeed in the space-frequency domain, a function like that given by Eq. (72) is completely identified by the frequency value $k_n/(2L)$.

This suggests the idea of measuring the accuracy of the numerical eigenmodes by evaluating the corresponding Fourier transform and analyzing the corresponding space-frequency domain. If there were no errors a single peak (theoretically, a Dirac $\delta$ function) corresponding to the exact value $f_{\lambda_n}$ should be obtained in the space-frequency domain. Instead if the numerical eigenvector presents some errors, the corresponding Fourier transform will produce either a shifted peak, or some other peaks in addition to the principal one.

Effective algorithms for performing discrete Fourier transform are available: for instance, the fast Fourier trasform (FFT), see [28]. The sampling space-interval $\Delta x = L/N_p = 0.0004$ m determines the maximum space-frequency, the well-known Nyquist frequency, which can be correctly resolved: $f_{\lambda,\text{Nyquist}} = 1/(2\Delta x)$. In this case, $f_{\lambda,\text{Nyquist}} = 1250$ m$^{-1}$.

On the other hand, the interval between transformed points in the space-frequency domain, $\Delta f_\lambda$, depends on the number $N_p$ of space samples and on the sampling space interval: $\Delta f_\lambda = 1/(N_p \Delta x)$. For a given $\Delta x$, the accuracy which can be achieved, *i.e.* the space-frequency resolution, increases with $N_p$ because $\Delta f_\lambda$ becomes smaller; as a consequence, since for numerical efficiency, FFT algorithms are based on transforming a number of points $N_s$ which must be an exact power of 2, a simple way to increase the frequency resolution is found by choosing $N_s$ large enough, and padding with zeros the sampled signal: therefore it is possible to achieve a spacing of points in the space-frequency domain $\Delta f = 1/(N_s \Delta x)$.

Here $N_p = 5001$, and with the selection $N_s = 2^{15} = 32768$, the addition of $N_s - N_p$ zeros at the end of the sequence of the signal points allows to achieve $\Delta f_\lambda = 0.076$ m$^{-1}$. The sampling interval in the space-frequency domain results therefore rather small, with more than 13 samples in each 1 m$^{-1}$-wide range. So, the space-frequency resolution of the space spectrum is high. FFT has been performed with subroutine DFOUR1, extracted from [73].

For the sake of conciseness, only the 500 DOFs case was considered for the simply-supported beam, and, again, only the $V(x)$ component of the eigenmode has been taken into consideration: the corresponding eigenvectors were calculated, using both FEM and IGA models, and their values were taken on a set of $N_p = 5001$ equally spaced points along the beam span. Results are expressed as plots of the square root of the *normalized power spectrum* (denoted in the Figures by the symbol (NPS)$^{1/2}$) *vs.* the space-frequency, $f_\lambda$.

The numerical models produce good results for the first modes; of course, the higher the number of considered modes, the larger the error becomes. This happens first, when a shift on the frequency domain can be detected.

Analyses were performed adopting a number of modes almost equally spaced in the natural frequency space: mode 85 (corresponding to theoretical values $k_2 = 57$ and $f_\lambda = 14.25$ m$^{-1}$); mode 168 ($k_1 = 59$ and $f_\lambda = 14.75$ m$^{-1}$); mode 251 ($k_2 = 161$ and $f_\lambda = 40.25$ m$^{-1}$); mode 334 ($k_2 = 214$ and $f_\lambda = 53.50$ m$^{-1}$); mode 417 ($k_1 = 150$ and $f_\lambda = 37.50$ m$^{-1}$) and mode 499 ($k_2 = 319$ and $f_\lambda = 79.75$ m$^{-1}$).

For example, Figure 15 (a) represents the FFT results corresponding to mode 85, and was obtained by applying the transformation to the eigenvectors built with quadratic ($p = 2$) FEM and IGA models with $p = 2$ and $p = 5$.

The analytical peak, labeled by a grey arrow (or a purple one, in the color reproduction), is clearly represented, as well as a shift of the FEM space-frequency peak which is a measure of the numerical error of this model. Instead, both IGA models perform very well and their peaks match the theoretical one.

Figure 15 (b) is referred to mode 168; in this case both IGA with $p = 2$ and quadratic FEM models produce a significant shift of the space-frequency peak $f_\lambda$; in addition, the FEM model shows some other peaks, too. These represent other frequency components associated to that vibration mode, which can be thought of as numerical noise, since no physical meaning can be assigned to them. On the other hand, the IGA model with $p = 5$ still produces excellent results.

Looking at a higher mode, for example mode 251, FFT analysis, shown in Figure 16 (a), highlights a good performance of higher degree ($p = 5$) IGA model, while both quadratic FEM and IGA with $p = 2$ present several peaks in addition to the principal one.

Higher errors are presented in Figure 16 (b), mode 334, where only the IGA with $p = 5$ can detect the exact principal peak, but even in this case there are other peaks due to numerical errors. The performance of FEM and IGA with $p = 2$ is worse, and this shows that the corresponding eigenmodes are meaningless.

If the last part of the spectrum is considered, *e.g.* mode 414, which is plotted in Figure 17 (a), the numerical errors become higher and all models cannot detect the exact theoretical peak and present other small peaks, too. Finally, in
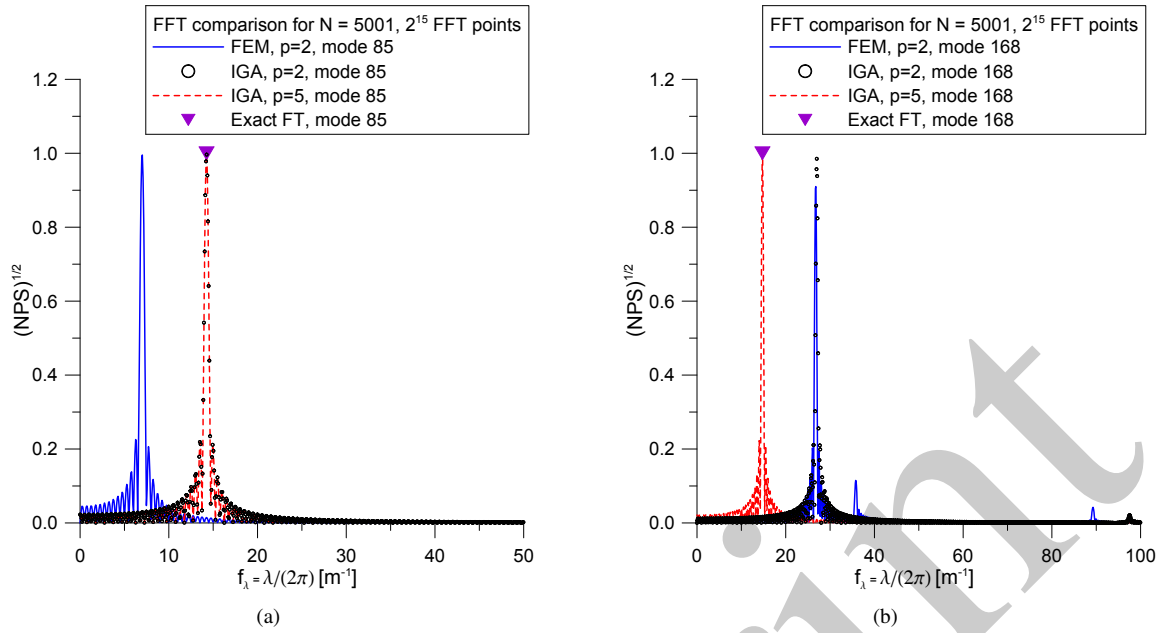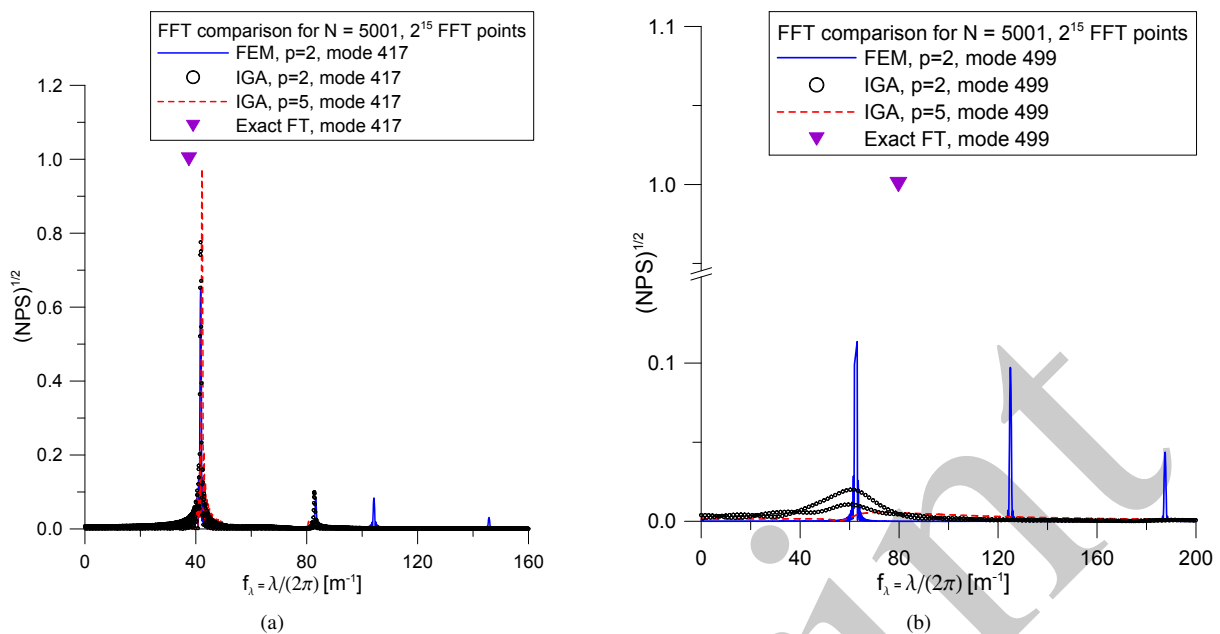
**Fig. 15** FFT of some eigenmodes almost equally spaced within the spectrum and numerically computed for the B22 Lagrangian finite element and IGA elements with order $p = 2$ and $p = 5$. (a) refers to mode 85: $k_2 = 57$ and $f_\lambda = 14.25$ m$^{-1}$; (b) to mode 168: $k_1 = 59$ and $f_\lambda = 14.75$ m$^{-1}$.
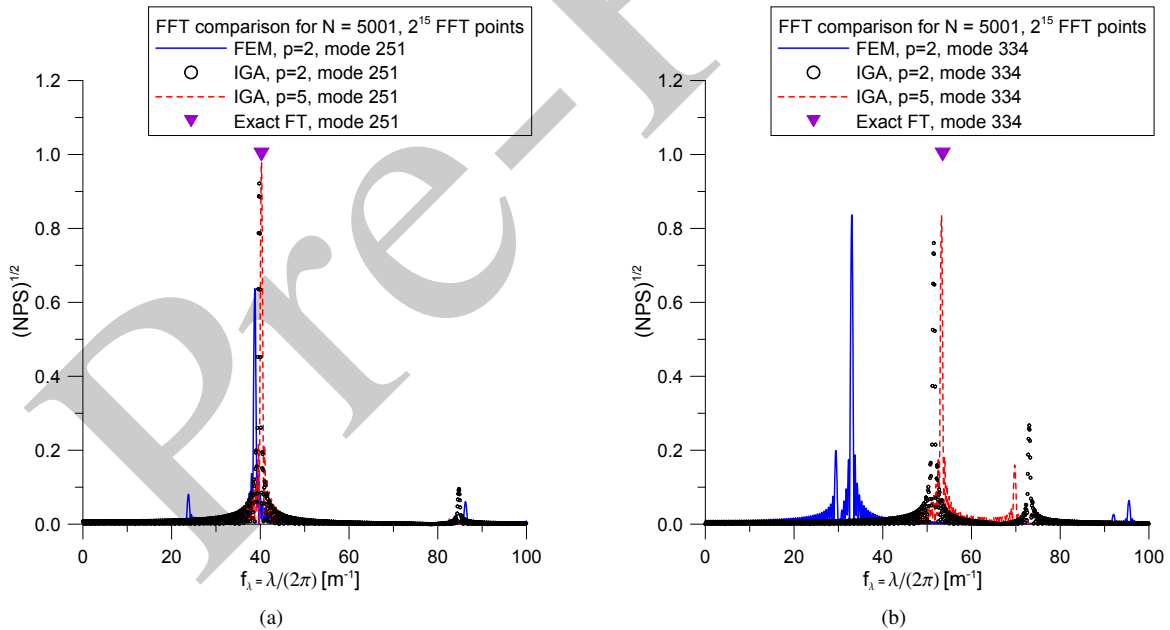


**Fig. 16** FFT of some eigenmodes almost equally spaced within the spectrum and numerically computed for the B22 Lagrangian finite element and IGA elements with order $p = 2$ and $p = 5$. (a) refers to mode 251: $k_2 = 161$ and $f_\lambda = 40.25$ m$^{-1}$; (b) to mode 334: $k_2 = 214$ and $f_\lambda = 53.50$ m$^{-1}$.

Figure 17 (b) the FFT of the *outlier* mode 499 is presented: both IGA models produce severe errors and any peak can be hardly found. The FEM model still presents both a shifted principal peak and other two peaks without physical meaning, but its performance is poor. Hence, no model can predict even a rough approximation of the real eigenmode.

**Fig. 17** FFT of some eigenmodes almost equally spaced within the spectrum and numerically computed for the `B22` Lagrangian finite element and IGA elements with order $p = 2$ and $p = 5$. (a) refers to mode 417: $k_1 = 150$ and $f_\lambda = 37.50 \text{ m}^{-1}$; (b) to mode 499: $k_2 = 319$ and $f_\lambda = 79.75 \text{ m}^{-1}$.

## 6 Conclusion

A complete review of the equations of motion for the Timoshenko beam model has been presented, at the beginning of this paper, in the case of free vibrations. The fundamental result is that the vibration spectrum of a Timoshenko beam is unique, but consists of two parts, none of which can be, in principle, disregarded. Specific attention has been devoted to the special cases of a simply-supported and of a doubly clamped beam: they provide a rather simple but exhaustive enough representative view of the different independent combinations which can be formed with the four elementary constraints for a single span beam.

In the former case, the transcendental equation which provides the wave-numbers corresponding to natural frequencies is factorized, and this property produces vibration modes (excluding the transition frequency, whose eigenmode is characterized by a constant function) which have, in both part of the spectrum, a simple shape, consisting of an integer number of sine/cosine half-waves.

In the latter case, instead, the transcendental equation does not factorize, and this produces much more complicated vibration modes: in the first part of the spectrum, both circular and hyperbolic sine/cosine functions are combined in each eigenmode, while in the second part of it, there appears a combination of sine/cosine functions depending, however, on two different wave-numbers. Moreover the transition frequency is not, in general, part of the spectrum, for this and for all other combination of constraints, excluding the simply-supported case.

In the body of the paper, these theoretical results have been used to validate the eigenvalues and eigenvectors obtained by several finite element models: two of them are based on a standard implementation of Lagrangian-interpolated displacement (both linear and quadratic), while the remaining four are based on the isogeometric approach, with an approximation order ranging from quadratic ($p = 2$) to quintic ($p = 5$). The analysis has been performed, similarly to what had been already done in the literature for the Euler-Bernoulli beam model, by considering the whole spectrum generated by a given number of DOFs. In particular, for the simply-supported case, the spectra corresponding to 100, 500 and 1000 DOFs (and hence to 100, 500 and 1000 natural modes) have been considered, and this has allowed to confirm that also for this structural model the isogeometric approach provides more accurate results. For the doubly clamped beam, the difficulties in computing the theoretical natural frequencies have limited the analysis to the spectrum generated by 100 natural modes; however, with reference to the simply-supported case, the fundamental trends have been confirmed.

A further step, which had not been considered yet, for the Euler-Bernoulli beam model (where, however, natural frequencies are much better separated than in the Timoshenko one) has been tried here, in order to assess the quality of the computed eigenmodes. For this purpose, and limiting, for simplicity, attention to the simply-supported case and to the transversal displacement component only, the $l^2$ discrete relative error has allowed to detect for the different finite element

model the threshold (in terms of natural modes) above which the accuracy of the computed eigenmode deteriorates. By combining this piece of information with the already computed error in the constructed spectrum, the conscious user of the finite element method is given a method for globally assessing the quality of his/her models. Some useful clues about the resolution, in terms of the number $N$ of DOFs, which is necessary to use if results must be accurate up to the $n$-th vibration mode, are provided, too.

The results presented in this work could be used for an in-depth analysis of some current and more actual problems. For instance, the case of curved Timoshenko beams might be interesting and useful for technical applications, particularly the extension to the computational framework, by adopting the isogeometric approach; for 1D problems some recent contributions appeared [20–22, 27, 32, 45, 46]. Again, the use of highly-efficient discretisation techniques, such as those reported in [12, 19, 88] is promising: they provide more refined stress description and might therefore improve the accuracy of numerical results.

Geometric nonlinearities have to be considered, as well, *viz.* by using the suggestions presented in [42, 44, 74, 79, 80], while a complete dynamic approach for the generalized beam theory has been addressed in [39, 66–69, 72, 82] and in the references cited therein.

The Timoshenko beam model is a particularly simple model from the point of view of micro-mechanical analysis. Therefore, it can be thought of as a simple prototype for providing fruitful clues in view of the development of new and more refined mathematical models of continua. The interested readers will find many insight, looking at the current research trend on generalized continua and their applications, for example in [8, 9] where modeling of bones is addressed; in [6, 7, 18, 36, 40, 64, 90] for gradient models; in [29, 71] for 2nd gradient models; in [47, 60, 62] for multi-constituent materials and in [26] for some hints on non-local problems.

Pantographic problems, see [2,3,37,38,43,75,76] represent a link between higher-order continua and beam models which might suggest fruitful ideas; in particular the review paper [35] considers the dynamic case. Homogenization theories are treated in [25], graded materials in [4, 15] and micropolar continua in [5].

Finally, it has to be pointed out that an accurate evaluation of the spectrum is fundamental in problems which consider damage detection, see for example [1, 13, 14, 81] and references provided therein, or try to optimize the structural response of smart structures such as the large one described in [10, 17, 84].

# References

[1] G. Alessandrini, A. Bilotta, A. Morassi, and E. Turco, Computing volume bounds of inclusions by EIT measurements, Journal of Scientific Computing **33**(3), 293–312 (2007).

[2] J. J. Alibert and A. Della Corte, Second-gradient continua as homogenized limit of pantographic microstructured plates: a rigorous proof, Zeitschrift für Angewandte Mathematik und Physik (ZAMP) **66**, 2855–2870 (2015).

[3] J. J. Alibert, P. Seppecher, and F. dell'Isola, Truss modular beams with deformation energy depending on higher displacement gradients, Mathematics and Mechanics of Solids **8**(1), 51–73 (2003).

[4] H. Altenbach and V. A. Eremeyev, Direct approach-based analysis of plates composed of functionally graded materials, Archive of Applied Mechanics **78**(10), 775–794 (2008).

[5] H. Altenbach and V. A. Eremeyev, On the linear theory of micropolar plates, ZAMM - Journal of Applied Mathematics and Mechanics / Zeitschrift für Angewandte Mathematik und Mechanik **89**(4), 242–256 (2009).

[6] H. Altenbach and V. A. Eremeyev, On the shell theory on the nanoscale with surface stresses, International Journal of Engineering Science **49**(12), 1294–1301 (2011).

[7] J. Altenbach, H. Altenbach, and V. A. Eremeyev, On generalized Cosserat-type theories of plates and shells: a short review and bibliography, Archive of Applied Mechanics **80**(1), 73–92 (2010).

[8] U. Andreaus, I. Giorgio, and T. Lekszycki, A 2-D continuum model of a mixture of bone tissue and bio-resorbable material for simulating mass density redistribution under load slowly variable in time, ZAMM - Journal of Applied Mathematics and Mechanics / Zeitschrift für Angewandte Mathematik und Mechanik **94**(12), 978–1000 (2014).

[9] U. Andreaus, I. Giorgio, and A. Madeo, Modeling of the interaction between bone tissue and resorbable biomaterial as linear elastic materials with voids, Zeitschrift für Angewandte Mathematik und Physik (ZAMP) **66**(1), 209–237 (2015).

[10] U. Andreaus, M. Colloca, and D. Iacoviello, An optimal control procedure for bone adaptation under mechanical stimulus, Control Engineering Practice **20**(6), 575 – 583 (2012).

[11] A. V. Balakrishnan, M. A. Shubov, and C. A. Peterson, Spectral analysis of coupled Euler-Bernoulli and Timoshenko beam model, ZAMM - Journal of Applied Mathematics and Mechanics / Zeitschrift für Angewandte Mathematik und Mechanik **84**(5), 291–313 (2004).

[12] A. Bilotta, G. Formica, and E. Turco, Performance of a high-continuity finite element in three-dimensional elasticity, International Journal for Numerical Methods in Biomedical Engineering (Communications in Numerical Methods in Engineering) **26**, 1155–1175 (2010).

[13] A. Bilotta and E. Turco, A numerical study on the solution of the Cauchy problem in elasticity, International Journal of Solids and Structures **46**, 4451–4477 (2009).

[14] A. Bilotta and E. Turco, Numerical sensitivity analysis of corrosion detection, Mathematics and Mechanics of Solids pp. 1–17 (2014), DOI: 10.1177/1081286514560093.

[15] M. Bîrsan, H. Altenbach, T. Sadowski, V. A. Eremeyev, and D. Pietras, Deformation analysis of functionally graded beams by the direct approach, Composites Part B: Engineering **43**(3), 1315–1328 (2012).

[16] J. A. C. Bresse, Cours de Mécanique Appliquée — Première Partie (Mallet-Bachelier, Paris, 1859).

[17] F. Buffa, A. Cazzani, A. Causin, S. Poppi, G. M. Sanna, M. Solci, F. Stochino, and E. Turco, The Sardinia Radio Telescope: a comparison between close range photogrammetry and FE models, Mathematics and Mechanics of Solids pp. 1–22 (2015), DOI: 10.1177/1081286515616227.

[18] A. Carcaterra, F. dell'Isola, R. Esposito, and M. Pulvirenti, Macroscopic description of microscopically strongly inhomogenous systems: A mathematical basis for the synthesis of higher gradients metamaterials, Archive for Rational Mechanics and Analysis **218**(3), 1239–1262 (2015).

[19] A. Cazzani, E. Garusi, A. Tralli, and S. N. Atluri, A four-node hybrid assumed-strain finite element for laminated composite plates, Computers, Materials & Continua **2**, 23–38 (2005).

[20] A. Cazzani, M. Malagù, and E. Turco, Isogeometric analysis of plane-curved beams, Mathematics and Mechanics of Solids pp. 1–16 (2014), DOI:10.1177/1081286514531265.

[21] A. Cazzani, M. Malagù, and E. Turco, Isogeometric analysis: a powerful numerical tool for the elastic analysis of historical masonry arches, Continuum Mechanics and Thermodynamics **28**(1–2), 139–156 (2016).

[22] A. Cazzani, M. Malagù, E. Turco, and F. Stochino, Constitutive models for strongly curved beams in the frame of isogeometric analysis, Mathematics and Mechanics of Solids **21**(2), 182–209 (2016).

[23] A. Cazzani, F. Stochino, and E. Turco, On the whole spectrum of Timoshenko beams. Part I: a theoretical revisitation, Zeitschrift für Angewandte Mathematik und Physik (ZAMP) pp. 1–28 (2015), DOI:10.1007/s00033-015-0592-0.

[24] A. Cazzani, F. Stochino, and E. Turco, On the whole spectrum of Timoshenko beams. Part II: further applications, Zeitschrift für Angewandte Mathematik und Physik (ZAMP) pp. 1–19 (2015), DOI:10.1007/s00033-015-0596-9.

[25] A. Cecchi and N. Rizzi, Heterogeneous elastic solids: a mixed homogenization-rigidification technique, International Journal of Solids and Structures **38**(1), 29–36 (2001).

[26] N. Challamel, A. Kocsis, and C. M. Wang, Discrete and non-local elastica, International Journal of Non-Linear Mechanics **77**, 128–140 (2015).

[27] A. Chiozzi, M. Malagù, A. Tralli, and A. Cazzani, ArchNURBS: NURBS-based tool for the structural safety assessment of masonry arches in MATLAB, Journal of Computing in Civil Engineering pp. 1–11 (2015), DOI:10.1061/(ASCE)CP.1943-5487.0000481.

[28] E. Chu, Discrete and continuous Fourier transforms — Analysis, applications and fast algorithms (CRC Press, Boca Raton, FL, 2008).

[29] N. M. Cordero, S. Forest, and E. P. Busso, Second strain gradient elasticity of nano–objects, Journal of the Mechanics and Physics of Solids (2015), DOI: 10.1016/j.jmps.2015.07.012.

[30] J. A. Cottrell, T. J. R. Hughes, and Y. Bazilevs, Isogeometric Analysis: Toward Integration of CAD and FEA (Wiley, Chichester, 2009).

[31] J. A. Cottrell, A. Reali, Y. Bazilevs, and T. J. R. Hughes, Isogeometric analysis of structural vibrations, Computer Methods in Applied Mechanics and Engineering **195**(41–43), 5257–5296 (2006).

[32] M. Cuomo, L. Contrafatto, and L. Greco, A variational model based on isogeometric interpolation for the analysis of cracked bodies, International Journal of Engineering Science **80**, 173–188 (2014).

[33] Dassault Systèmes, ABAQUS 6.14 Documentation – Theory Guide, Providence, RI, 2015.

[34] C. de Falco, A. Reali, and R. Vàzquez, GeoPDEs: A research tool for isogeometric analysis of PDEs, Advances in Engineering Software **42**(12), 1020–1034 (2011).

[35] D. Del Vescovo and I. Giorgio, Dynamic problems for metamaterials: review of existing models and ideas for further research, International Journal of Engineering Science **80**, 153–172 (2014).

[36] F. dell'Isola, U. Andreaus, and L. Placidi, At the origins and in the vanguard of peridynamics, non-local and higher-gradient continuum mechanics: An underestimated and still topical contribution of Gabrio Piola, Mathematics and Mechanics of Solids **20**(8), 887–928 (2015).

[37] F. dell'Isola, A. Della Corte, I. Giorgio, and D. Scerrato, Pantographic 2D sheets: discussion of some numerical investigations and potential applications, International Journal of Non-Linear Mechanics (2015), DOI:10.1016/j.ijnonlinmec.2015.10.010.

[38] F. dell'Isola, T. Lekszycki, M. Pawlikowski, R. Grygoruk, and L. Greco, Designing a light fabric metamaterial being highly macroscopically tough under directional extension: first experimental evidence, Zeitschrift für Angewandte Mathematik und Physik (ZAMP) pp. 1–26 (2015), DOI:10.1007/s00033-015-0556-4.

[39] F. dell'Isola, A. Madeo, and L. Placidi, Linear plane wave propagation and normal transmission and reflection at discontinuity surfaces in second gradient 3d continua, ZAMM - Journal of Applied Mathematics and Mechanics / Zeitschrift für Angewandte Mathematik und Mechanik **92**(1), 52–71 (2012).

[40] F. dell'Isola, P. Seppecher, and A. Della Corte, The postulations á la D'Alembert and á la Cauchy for higher gradient continuum theories are equivalent: a review of existing results, Proceedings of the Royal Society of London A: Mathematical, Physical and Engineering Sciences **471**(2183), 1–25 (2015), DOI: 10.1098/rspa.2015.0415.

[41] I. Elishakoff, J. Kaplunov, and E. Nolde, Celebrating the centenary of Timoshenko's study of effects of shear deformation and rotary inertia, Applied Mechanics Reviews **67**(12), 060802–1–11 (2015).

[42] S. Gabriele, N. Rizzi, and V. Varano, A 1D higher gradient model derived from Koiter's shell theory, Mathematics and Mechanics of Solids pp. 1–10 (2014), DOI: 10.1177/1081286514536721.

[43] I. Giorgio, R. Grygoruk, F. dell'Isola, and D. J. Steigmann, Pattern formation in the three-dimensional deformations of fibered sheets, Mechanics Research Communications 69, 164–171 (2015).

[44] L. Greco and M. Cuomo, On the force density method for slack cable nets, International Journal of Solids and Structures 49(13), 1526 – 1540 (2012).

[45] L. Greco and M. Cuomo, B-Spline interpolation of Kirchhoff–Love space rods, Computer Methods in Applied Mechanics and Engineering 256, 251–269 (2013).

[46] L. Greco and M. Cuomo, An implicit $G^1$ multi patch B-spline interpolation for Kirchhoff-Love space rod, Computer Methods in Applied Mechanics and Engineering 269, 173–197 (2014).

[47] A. Grillo, S. Federico, and G. Wittum, Growth, mass transfer, and remodeling in fiber-reinforced, multi-constituent materials, International Journal of Non-Linear Mechanics 47(2), 388–401 (2012).

[48] M. Hajianmaleki and M. S. Qatu, Static and vibration analyses of thick, generally laminated deep curved beams with different boundary conditions, Composites Part B: Engineering 43(4), 1767–1775 (2012).

[49] M. Hajianmaleki and M. S. Qatu, Vibrations of straight and curved composite beams: A review, Composite Structures 100, 218–232 (2013).

[50] S. M. Han, H. Benaroya, and T. Wei, Dynamics of transversely vibrating beams using four engineering theories, Journal of Sound and Vibration 225, 935–988 (1999).

[51] E. Hernández and E. Otárola, A superconvergent scheme for a locking-free FEM in a Timoshenko optimal control problem, ZAMM - Journal of Applied Mathematics and Mechanics / Zeitschrift für Angewandte Mathematik und Mechanik 91(4), 288–299 (2011).

[52] T. J. R. Hughes, The finite element method: linear static and dynamic finite element analysis (Prentice-Hall, Inc., Englewood Cliffs, NJ, 1987).

[53] T. J. R. Hughes, J. A. Cottrell, and Y. Bazilevs, Isogeometric analysis: CAD, finite elements, NURBS, exact geometry and mesh refinement, Computer Methods in Applied Mechanics and Engineering 194(39–41), 4135–4195 (2005).

[54] T. J. R. Hughes, J. A. Evans, and A. Reali, Finite element and NURBS approximations of eigenvalue, boundary-value, and initial-value problems, Computer Methods in Applied Mechanics and Engineering 272(04), 290–320 (2014).

[55] T. J. R. Hughes, H. M. Hilber, and R. L. Taylor, A reduction scheme for problems of structural dynamics, International Journal of Solids and Structures 12(11), 749–767 (1976).

[56] C. Lanczos, An iteration method for the solution of the eigenvalue problem of linear differential and integral operators, Journal of Research of the National Bureau of Standards 45, 225–282 (1950).

[57] S. J. Lee and K. S. Park, Vibrations of Timoshenko beams with isogeometric approach, Applied Mathematical Modelling 37(22), 9174–9190 (2013).

[58] A. T. Luu, N. I. Kim, and J. Lee, Isogeometric vibration analysis of free-form Timoshenko curved beams, Meccanica 50(1), 169–187 (2015).

[59] A. T. Luu, N. I. Kim, and J. Lee, NURBS-based isogeometric vibration analysis of generally laminated deep curved beams with variable curvature, Composite Structures 119, 150–165 (2015).

[60] A. Madeo, L. Placidi, and G. Rosi, Towards the design of metamaterials with enhanced damage sensitivity: Second gradient porous materials, Research in Nondestructive Evaluation 25(2), 99–124 (2014).

[61] MathWorks, MATLAB 2013.a Documentation, Natick, MA, 2013.

[62] A. Misra and P. Poorsolhjouy, Granular micromechanics model for damage and plasticity of cementitious materials based upon thermomechanics, Mathematics and Mechanics of Solids (2015), DOI:10.1177/1081286515576821.

[63] C. B. Moler and G. W. Stewart, An algorithm for generalized matrix eigenvalue problems, SIAM Journal on Numerical Analysis 10(2), 241–256 (1974).

[64] P. Neff, I. D. Ghiba, A. Madeo, L. Placidi, and G. Rosi, A unifying perspective: the relaxed linear micromorphic continuum, Continuum Mechanics and Thermodynamics 26(5), 639–681 (2014).

[65] L. C. Pagnini and G. Piccardo, The three-hinged arch as an example of piezomechanic passive controlled structure, Continuum Mechanics and Thermodynamics pp. 1–16 (2015), 10.1007/s00161-015-0474-x.

[66] G. Piccardo, L. C. Pagnini, and F. Tubino, Some research perspectives in galloping phenomena: critical conditions and post-critical behavior, Continuum Mechanics and Thermodynamics 27(1-2), 261–285 (2015).

[67] G. Piccardo, G. Ranzi, and A. Luongo, A complete dynamic approach to the generalized beam theory cross-section analysis including extension and shear modes, Mathematics and Mechanics of Solids 19(8), 900–924 (2014).

[68] G. Piccardo, G. Ranzi, and A. Luongo, A direct approach for the evaluation of the conventional modes within the {GBT} formulation, Thin-Walled Structures 74, 133–145 (2014).

[69] G. Piccardo, F. Tubino, and A. Luongo, A shear–shear torsional beam model for nonlinear aeroelastic analysis of tower buildings, Zeitschrift für Angewandte Mathematik und Physik (ZAMP) 66(4), 1895–1913 (2015).

[70] L. Piegl and W. Tiller, The NURBS Book, 2nd edition (Springer-Verlag, Berlin-Heidelberg, 1997).

[71] L. Placidi, A variational approach for a nonlinear 1-dimensional second gradient continuum damage model, Continuum Mechanics and Thermodynamics 27(4), 623–638 (2015).

[72] L. Placidi, G. Rosi, I. Giorgio, and A. Madeo, Reflection and transmission of plane waves at surfaces carrying material properties and embedded in second-gradient materials, Mathematics and Mechanics of Solids (2013), DOI: 10.1177/1081286512474016.

[73] W. H. Press, S. A. Teukolsky, W. T. Vetterling, and B. P. Flannery, Numerical Recipes in Fortran — The art of scientific computing, 2nd edition (Cambridge University Press, New York, 1992).

[74] F. Presta, C. R. Hendy, and E. Turco, Numerical validation of simplified theories for design rules of transversely stiffened plate girders, The Structural Engineer **86**(21), 37–46 (2008).

[75] Y. Rahali, I. Giorgio, J. F. Ganghoffer, and F. dell'Isola, Homogenization à la Piola produces second gradient continuum models for linear pantographic lattices, International Journal of Engineering Science **97**, 148–172 (2015).

[76] Y. Rahali, I. Goda, and J. F. Ganghoffer, Numerical identification of classical and nonclassical moduli of 3d woven textiles and analysis of scale effects, Composite Structures **135**, 122–139 (2016), DOI:10.1016/j.compstruct.2015.09.023.

[77] G. V. Rao and K. K. Raju, Large amplitude free vibrations of beams — an energy approach, ZAMM - Journal of Applied Mathematics and Mechanics / Zeitschrift für Angewandte Mathematik und Mechanik **83**(7), 493–498 (2003).

[78] A. Reali, An isogeometric analysis approach for the study of structural vibrations, Journal of Earthquake Engineering **10**, 1–30 (2006).

[79] N. Rizzi and V. Varano, The effects of warping on the postbuckling behaviour of thin-walled structures, Thin-Walled Structures **49**(9), 1091–1097 (2011).

[80] N. Rizzi, V. Varano, and S. Gabriele, Initial postbuckling behavior of thin-walled frames under mode interaction, Thin–Walled Structures **68**, 124–134 (2013).

[81] N. Roveri and A. Carcaterra, Damage detection in structures under travelling loads by the Hilbert-Huang transform, Mechanical System and Signal Processing **28**, 128–144 (2012).

[82] G. Solari, L. C. Pagnini, and G. Piccardo, A numerical algorithm for the aerodynamic identification of structures, Journal of Wind Engineering and Industrial Aerodynamics **69–71**, 719–730 (1997).

[83] J. Stefan, Über die Transversalschwingungen eines elastischen Stabes (K. K. Hof- und Staatsdruckerei, Wien, 1858).

[84] F. Stochino, A. Cazzani, S. Poppi, and E. Turco, Sardinia Radio Telescope finite element model updating by means of photogrammetric measurements, Mathematics and Mechanics of Solids pp. 1–17 (2015), DOI: 10.1177/1081286515616046.

[85] J. W. Strutt (Baron Rayleigh), The Theory of Sound — Vol. 1 (Macmillan and Co., London, 1877).

[86] S. P. Timoshenko, On the correction for shear of the differential equation for transverse vibrations of prismatic bars, Philosophical Magazine (Series 5) **41**, 744–746 (1921).

[87] S. P. Timoshenko, On the transverse vibrations of bars of uniform cross-section, Philosophical Magazine (Series 5) **43**, 125–131 (1922).

[88] E. Turco and P. Caracciolo, Elasto-plastic analysis of Kirchhoff plates by high simplicity finite elements, Computer Methods in Applied Mechanics and Engineering **190**, 691–706 (2000).

[89] O. Weeger, U. Wever, and B. Simeon, Isogeometric analysis of nonlinear Euler-Bernoulli beam vibrations, Nonlinear Dynamics **72**(4), 813–835 (2013).

[90] Y. Yang, W. Ching, and A. Misra, Higher-order continuum theory applied to fracture simulation of nanoscale intergranular glassy film, Journal of Nanomechanics and Micromechanics **1**(2), 60–71 (2011).